

# Can an Anti-de Sitter Vacuum in the Dark Energy Sector Explain JWST High-Redshift Galaxy and Reionization Observations?

Anirban Chakraborty,<sup>a,1</sup> Tirthankar Roy Choudhury,<sup>a</sup> Anjan Ananda Sen,<sup>b</sup> and Purba Mukherjee<sup>b</sup>

<sup>a</sup>National Centre for Radio Astrophysics, Tata Institute of Fundamental Research, Pune University Campus, Ganeshkhind, Pune 411007, India.

<sup>b</sup>Centre for Theoretical Physics, Jamia Millia Islamia, New Delhi-110025, India.

E-mail: [anirban@ncra.tifr.res.in](mailto:anirban@ncra.tifr.res.in), [tirth@ncra.tifr.res.in](mailto:tirth@ncra.tifr.res.in), [aasen@jmi.ac.in](mailto:aasen@jmi.ac.in), [pdf.p Mukherjee@jmi.ac.in](mailto:pdf.p Mukherjee@jmi.ac.in)

**Abstract.** The James Webb Space Telescope’s (JWST) discovery of an unexpectedly high abundance of UV-bright galaxies at redshifts  $z > 10$  poses a significant challenge to the standard  $\Lambda$ CDM cosmology. This work tests whether this tension can be resolved **solely** by modifying the cosmological background, without invoking significant evolution in the astrophysical properties of early galaxies. We investigate an alternative framework featuring the presence of an anti-de Sitter vacuum in the dark energy sector, a model that naturally arises in quantum gravity models like string theory and can enhance early structure formation. Using a self-consistent semi-analytical model that couples galaxy evolution with reionization, we confront this scenario with a wide range of observations. We first show that while a model tailored to fit the high- $z$  UV luminosity functions (UVLFs) shows promise, it is in *strong tension* with well-established cosmological constraints from the CMB and other low-redshift probes. Conversely, models within this framework that *are* consistent with these constraints provide only a modest boost to structure formation and *fail to reproduce* the observed JWST galaxy abundances at  $z > 10$ . While these models remain consistent with the cosmic reionization history, our primary result is that this class of cosmological modifications is insufficient on its own to explain the galaxy excess. Our study underscores the critical importance of holistic testing for any beyond- $\Lambda$ CDM proposal; apparent success in one observational regime does not guarantee overall viability. By demonstrating the limitations of a purely cosmological solution, our results strengthen the case that evolving astrophysical properties are a necessary ingredient for solving the challenge of early galaxy formation.

**Keywords:** dark energy theory, high redshift galaxies, semi-analytic modeling, reionization

---

<sup>1</sup>Corresponding author.

---

## Contents

<b>1</b>	<b>Introduction</b>	<b>1</b>
<b>2</b>	<b>Theoretical Formalism</b>	<b>2</b>
2.1	Cosmological Model: Structure formation and Halo statistics	2
2.1.1	Background Cosmological Evolution	2
2.1.2	Abundance of Collapsed Objects	3
2.2	Astrophysical Model: Populating halos with UV Galaxies	6
<b>3</b>	<b>Observational Datasets and Likelihood Analysis</b>	<b>9</b>
<b>4</b>	<b>Results and Discussion</b>	<b>11</b>
4.1	A fiducial model: success with JWST, tension with the CMB	11
4.2	A viable $\text{CPL}n\Lambda\text{CDM}$ model exhibiting maximum boost in halo abundance (relative to $\Lambda\text{CDM}$ ) at high redshifts ( $z \approx 13.2$ )	15
<b>5</b>	<b>Conclusion</b>	<b>20</b>
<b>A</b>	<b>Constraints on the redshift evolution of galaxy properties from JWST UVLF observations in the <math>\Lambda\text{CDM}</math> cosmological framework</b>	<b>22</b>
<b>B</b>	<b>Constraints on the cosmological parameters in the <math>\text{CPL}n\Lambda\text{CDM}</math> cosmology, as obtained by Mukherjee et al. (2025)</b>	<b>24</b>
<b>C</b>	<b>A <math>\text{CPL}n\Lambda\text{CDM}</math> model that maximizes the boost in halo abundance (relative to <math>\Lambda\text{CDM}</math>) at <math>z \approx 13.2</math> compared to <math>z \approx 5</math></b>	<b>25</b>

---

## 1 Introduction

The standard Lambda Cold Dark Matter ( $\Lambda\text{CDM}$ ) model is the cornerstone of modern cosmology, successfully explaining a vast range of phenomena from the cosmic microwave background (CMB) to the late-time acceleration of the Universe [1–20]. However, this paradigm is facing a significant new challenge from the early Universe. Observations with the James Webb Space Telescope (JWST) have revealed a surprising abundance of luminous galaxies at redshifts  $z \gtrsim 10$  [21–41]. The number density of these objects significantly exceeds predictions from canonical  $\Lambda\text{CDM}$ -based models [42–44]. Because the abundance of early galaxies encodes crucial information about the growth of the first cosmic structures, this discrepancy offers a powerful test of the underlying cosmological framework.

Two primary pathways have emerged to explain these observations. The first proposes modifications to astrophysical processes, including: (*i*) an enhanced efficiency or stochasticity of star formation [45–56]; (*ii*) a top-heavy stellar initial mass function [34, 57–62]; (*iii*) minimal dust attenuation at early times [63–66]; or (*iv*) a significant contribution from accreting black holes [57, 67–69].

Complementing these proposals, a second pathway considers whether the tension points to a flaw in the standard cosmology itself. This has motivated explorations of beyond- $\Lambda\text{CDM}$  physics aimed at enhancing early structure formation. Efforts include invoking early

dark energy [70, 71], exotic dark matter candidates [72, 73], primordial black holes [74–77], or alterations to the primordial power spectrum and matter transfer function [78–81]. While appealing, the viability of some of these cosmological solutions remains highly debated [82, 83].

In this work, we focus on modifications to the dark energy sector, which affects the cosmic expansion history  $H(z)$ . The rate of expansion sets the Hubble drag, which resists the gravitational collapse of density perturbations into the halos that host galaxies [84–87]. While the positive cosmological constant in  $\Lambda$ CDM successfully drives late-time acceleration, it is plagued by theoretical issues like the fine-tuning and coincidence problems [88, 89]. Furthermore, constructing a stable, positive vacuum energy (a de Sitter vacuum) is notoriously difficult within string theory [90–96]. In contrast, potentials featuring a negative minimum, an Anti-de Sitter (AdS) vacuum, arise more naturally [97]. Consequently, in the literature, cosmological models featuring a composite dark energy sector with a negative cosmological constant ( $\Lambda < 0$ ), supplemented by a dynamical scalar field ( $\phi$ ), have been advanced as attractive alternatives that can satisfy the late-time acceleration constraints as well as remain consistent with other low redshift cosmological observations [98–108].

Recent studies have even shown that such models can enhance high-redshift structure formation, making them promising candidates for explaining the JWST galaxy excess [105, 109, 110]. As cosmic reionization is driven by these same galaxy populations, any modification to their abundance will necessarily impact the ionization state of the intergalactic medium (IGM) [111–115].

Therefore, our primary objective is to perform a rigorous and *simultaneous* test of this theoretically motivated cosmological scenario. We investigate whether a model with a negative cosmological constant can *alone* reproduce the observed abundance of UV-luminous galaxies across the redshift range  $5 \leq z < 14$  *and* satisfy the constraints on cosmic reionization. By demanding that the solution works without any evolution in the astrophysical properties of galaxies, we subject this cosmological framework to its most stringent possible test.

This paper is organized as follows. In Section 2, we detail our theoretical framework. Section 3 summarizes the observational datasets and our analysis methodology. We present and discuss our results in Section 4 and conclude in Section 5. Unless stated otherwise, we adopt the best-fit cosmological parameters from the Planck 2018 analysis for the baseline  $\Lambda$ CDM model [6]:  $\Omega_m = 0.3158$ ,  $\Omega_{DE} = 0.6841077$ ,  $\Omega_r = 9.23 \times 10^{-5}$ ,  $\Omega_b = 0.0493$ ,  $h = 0.6732$ ,  $\sigma_8 = 0.8120$  and  $n_s = 0.96605$ .

## 2 Theoretical Formalism

### 2.1 Cosmological Model: Structure formation and Halo statistics

In this subsection, we describe the background cosmological model and the framework for tracking the growth of matter perturbations and calculating other cosmological quantities, such as the halo mass function, which serves as input to the galaxy formation and evolution model discussed in the next subsection.

#### 2.1.1 Background Cosmological Evolution

We assume a spatially flat, homogeneous, and isotropic Universe comprising radiation, non-relativistic matter, and dark energy. For the dark energy sector, we consider an evolving dark energy component, modelled as a rolling scalar field ( $\phi$ ), in the presence of a cosmological

constant  $\Lambda$ , which is negative [104, 105, 110]. We adopt one of the most widely used parameterizations, known as the Chevallier-Polarski-Linder (CPL) parameterization [116, 117], to describe the equation of state,  $w_\phi = P_\phi/\rho_\phi$ , for the field  $\phi$ , which varies with redshift  $z$  -

$$w_\phi(z) = w_0 + w_a \left( \frac{z}{1+z} \right) \quad (2.1)$$

where  $w_0$  and  $w_a$  are constants determining the value of the equation of state and its rate of change (with respect to the scale factor) at the present epoch, respectively. As per the above parameterization, the equation of state smoothly evolves from a value of  $w_\phi = w_0$  at  $z = 0$  to  $w_\phi \rightarrow w_0 + w_a$  as  $z \rightarrow \infty$ .

Assuming a spatially flat Universe, the first Friedmann equation, which describes the evolution of the Hubble expansion rate, can be written as -

$$H^2(z) = H_0^2 \left[ \Omega_r(1+z)^4 + \Omega_m(1+z)^3 + \Omega_\Lambda + \Omega_\phi(1+z)^{3(1+w_0+w_a)} \exp \left( -3w_a \frac{z}{1+z} \right) \right] \quad (2.2)$$

where  $H_0$  is the Hubble constant and  $\Omega_i$  is the present-day density parameter of the  $i$ -th component, such as radiation, matter, a cosmological constant, and the scalar field  $\phi$ .

From equation (2.2), it is clear that larger values of  $w_0$  and  $w_a$  lead to greater dark energy density, and result in a higher rate of cosmic expansion  $H(z)$ .

We identify the total dark energy (DE) sector as comprising the CPL scalar field with density parameter  $\Omega_\phi$ , and the cosmological constant component with density parameter  $\Omega_\Lambda$ . Therefore, it immediately follows that

$$\Omega_{\text{DE}} = \Omega_\phi + \Omega_\Lambda = 1 - \Omega_m - \Omega_r \quad (2.3)$$

It is important to realize that we only need the *total* dark energy density to be positive at the low redshifts and satisfy the current observational constraints on the amount of dark energy (i.e.,  $\Omega_{\text{DE}} \approx 0.68$ ) in order to account for the late-time accelerated expansion of the Universe [6]. This implies that  $\Omega_\Lambda$  is in principle free to assume any value (positive and negative), thereby allowing for a wide variety of possibilities within the *total* dark energy sector.

From these discussions, it follows that the cosmological parameters -  $(w_0, w_a, \Omega_\Lambda)$  completely characterize the dynamics of the dark energy sector within our cosmological model. In our formalism, the standard  $\Lambda$ CDM cosmology corresponds to the case -  $w_0 = -1, w_a = 0, \Omega_\Lambda = 0$  (i.e.,  $\Omega_\phi = \Omega_{\text{DE}}$ ).

### 2.1.2 Abundance of Collapsed Objects

Having specified the background cosmology, we now move towards studying the formation of collapsed objects and their statistical properties at a given cosmic epoch in such a Universe.

The dark matter halo mass function, which describes the number of dark matter halos per unit comoving volume at redshift  $z$  with masses between  $M_h$  and  $M_h + dM_h$ , can be expressed as follows [85–87]-

$$\frac{dn}{dM_h}(M_h, z) = -\frac{\bar{\rho}_m}{M_h} \frac{d \ln \sigma(M_h, z)}{dM_h} f[\sigma(M_h, z)] \quad (2.4)$$

where  $\bar{\rho}_m$  is the mean comoving background matter density,  $\sigma(M_h, z)$  is the variance of matter density fluctuations smoothed on the comoving scale  $R = (3M_h/4\pi\bar{\rho})^{1/3}$ . The mass variance  $\sigma(M_h, z)$  is related to the linearly-extrapolated power spectrum of matter density fluctuations  $P_L(k, z)$  as follows,

$$\sigma^2(M_h, z) = \frac{1}{2\pi^2} \int_0^\infty dk k^2 P_L(k, z) \hat{W}^2(k, R) \quad (2.5)$$

In the above expression,  $\hat{W}(k, R) = 3[\sin(kR) - kR \cos(kR)]/(kR)^3$  is the Fourier transform of the real-space spherical top-hat window function of radius  $R$ . The linearly-extrapolated power spectrum  $P_L(k, z)$  of matter density fluctuations as a function of wavenumber  $k$  at a given redshift  $z$  can further be expressed as:

$$P_L(k, z) = P_0 k^{n_s} T^2(k) D^2(z) \quad (2.6)$$

where  $P_0$  is a normalization constant, which is fixed using the present-day mass variance ( $\sigma_8$ ) on a scale of  $8 h^{-1}\text{cMpc}$ ,  $T(k)$  is the matter transfer function, and  $D(z)$  is the linear growth factor. Throughout this work, we normalize the growth factor to  $D(z=0) = 1$ . We use the Sheth & Tormen formalism [118] for calculating the halo mass function, wherein the function  $f[\sigma(M_h, z)]$  is given as

$$f(\sigma) = A \sqrt{\frac{2a}{\pi}} \left[ 1 + \left( \frac{\sigma^2(M_h, z)}{a\delta_c^2} \right)^p \right] \frac{\delta_c}{\sigma(M_h, z)} \exp \left[ -\frac{a\delta_c^2}{2\sigma^2(M_h, z)} \right], \quad (2.7)$$

with  $\delta_c = 1.686$  representing the critical linear overdensity for collapse. The parameters  $(A, a, p)$  are set to the values obtained in Jenkins et al. (2001) [119], namely  $A = 0.353$ ,  $a = 0.73$ , and  $p = 0.175$ . We use the transfer function,  $T(k)$ , introduced by Eisenstein and Hu [120] in our calculations.

A key ingredient for calculating the halo mass function is the linear growth factor of density perturbations  $D(z)$ , which determines how density perturbations evolve with redshift in a given cosmological model and is defined in terms of the perturbation amplitude as  $D(z) \equiv \delta(z)/\delta(z=0)$ .

We compute the growth factor by numerically solving the second-order differential equation below, which describes the growth of matter density perturbations on sub-Hubble length scales in the linear regime :

$$\delta'' + \left[ \frac{3}{a} + \frac{E'(a)}{E(a)} \right] \delta' - \frac{3}{2} \frac{\Omega_m}{a^5 E^2(a)} \delta = 0, \quad (2.8)$$

where  $'$  indicates a derivative with respect to the scale factor  $a (\equiv 1/z - 1)$ , and  $E(a) \equiv H(a)/H_0$  denotes the normalized expansion rate. The last term on the left-hand side of the above equation represents the gravitational source term, which facilitates the growth of perturbations via the process of gravitational instability, while the second term on the left-hand side corresponds to the Hubble friction term, which tends to suppress their growth due to the expansion of the Universe. The interplay between these competing effects governs the overall rate of structure formation.

Therefore, one can easily see that cosmological models with dynamical dark energy not only alter the background expansion rate (equation (2.2)) but also directly affect the growth of

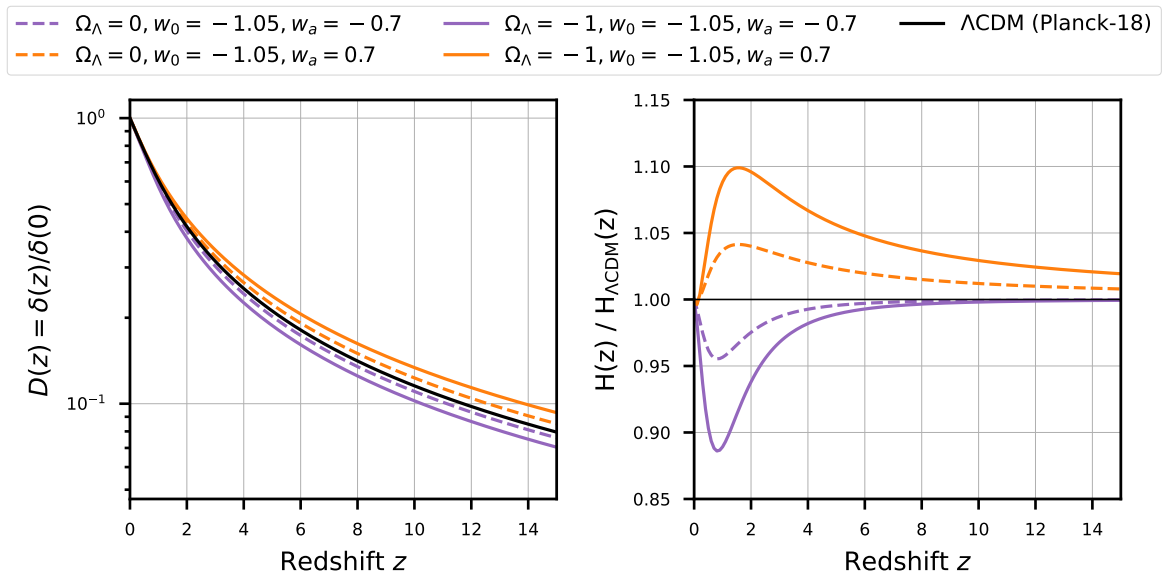


**Figure 1:** The evolution of the linear growth factor (left panel) and the Hubble expansion rate  $H(z)$  relative to  $\Lambda$ CDM (right panel) as a function of redshift for different cosmological models with dynamical dark energy.

large-scale structures (via modifications to  $E(z)$  in equation (2.8)). We solve equation (2.8) numerically for a given cosmological model, with the initial conditions -  $\delta(a_i) = a_i$  and  $\delta'(a_i) = 1$  at some initial scale factor  $a_i = 10^{-3}$  [105].

Before proceeding further, let us examine how cosmological models with dynamical dark energy affect the growth of density perturbations and the halo mass function. We only vary the parameters governing the *total* dark energy sector, while keeping all other cosmological parameters such as  $H_0$ ,  $\Omega_m$  fixed to their **Planck 2018** best-fit values, as specified at the end of Section 1. For illustration, we select a class of cosmological models, where the evolving CPL component is in the phantom regime at present having  $w_\phi < -1$  (i.e.,  $w_0 < -1$ ) but is free to either remain in the phantom regime with  $w_\phi < -1$  (i.e.,  $w_0 + w_a < -1$ ) or transition to the non-phantom regime with  $w_\phi > -1$  (i.e.,  $w_0 + w_a > -1$ ) at higher redshifts depending on how quickly  $w_\phi$  changes with time (i.e., the sign and value of  $w_a$ ). We show the redshift evolution of the linear growth factor  $D(z)$  and the Hubble expansion rate  $H(z)$  for such models in the different panels of Figure 1. It follows from equation (2.8) that a faster expansion rate compared to the  $\Lambda$ CDM model suppresses the growth of matter perturbations due to increased Hubble friction. When normalized to produce the same amplitude of perturbations today, this leads to larger growth factors at earlier epochs, as shown in the left panel of Figure 1. By similar arguments, models that exhibit an expansion rate slower than the  $\Lambda$ CDM yield smaller growth factors. The inclusion of a negative cosmological constant only aggravates the impact on the growth factor at high redshifts since a more negative  $\Lambda$  (i.e., a larger value of  $|\Omega_\Lambda|$ ) demands a correspondingly larger positive energy density contribution from the CPL component ( $\Omega_\phi$ ) to satisfy observational constraints on late-time acceleration—namely, that  $\Omega_\Lambda + \Omega_\phi \simeq 0.68$  (see equation (2.3)).

In Figure 2, we show the impact of increasingly negative values of the cosmological constant in the dark energy sector (alongside an evolving CPL component having fiducial

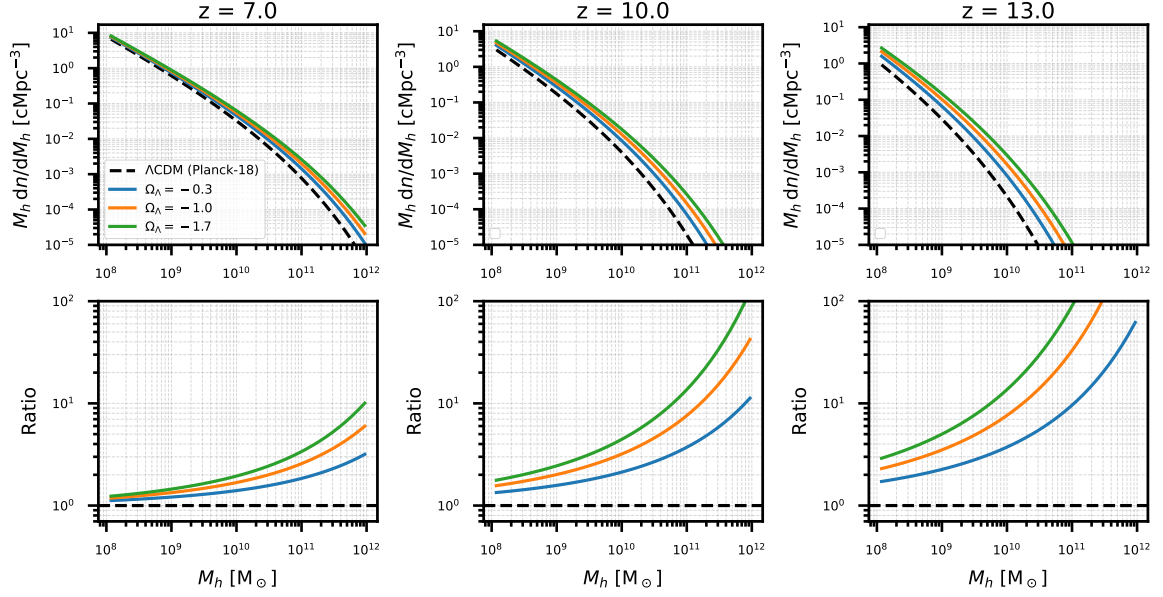


**Figure 2:** The effect of dynamical dark energy models, featuring a scalar field with a redshift-dependent equation of state described by equation (2.1) and a negative cosmological constant  $\Lambda$ , on the dark matter halo mass functions at high redshifts ( $z = 7, 10$ , and  $13$ ). Here, we vary  $\Omega_\Lambda$  while keeping the equation of state parameters of the scalar field fixed ( $w_0 = -1.05$ ,  $w_a = 0.7$ ).

values of  $w_0 = -1.05$  and  $w_a = 0.7$ ) on the halo mass function at  $z > 6$ . As previously discussed, a more negative cosmological constant necessitates a proportionally higher energy density in the evolving CPL component ( $\Omega_\phi$ ), which in turn further enhances the growth factor at earlier times, ultimately leading to a pronounced boost in the halo mass function. In the cosmological models chosen for illustration in Figure 2, we find that the abundance of dark matter halos of a fixed mass compared to the  $\Lambda$ CDM model systematically increases as one moves towards higher redshifts.

## 2.2 Astrophysical Model: Populating halos with UV Galaxies

In this subsection, we present the astrophysical framework of our theoretical model, outlining the prescriptions used to model star formation activity and ionizing photon production in high-redshift galaxies, as well as the methodology used to compute various global observables associated with galaxy populations and cosmic reionization. We use the framework described in our earlier works [48, 49] (hereafter, CC24 and CC25), which self-consistently models the evolving UV luminosity function (UVLF) of galaxies and the global reionization history while incorporating the effects of radiative feedback. We present a brief summary of the main features of the model below, and refer interested readers to CC24 and CC25 for further details.

In this model, the star-formation rate  $\dot{M}_*$  of a galaxy residing within a halo of mass  $M_h$  is calculated as

$$\dot{M}_*(M_h, z) = \frac{f_*(M_h, z)}{t_*(z)} f_{\text{gas}}(M_h) \left( \frac{\Omega_b}{\Omega_m} \right) M_h, \quad (2.9)$$



where,  $f_*(M_h, z)$  represents the star-formation efficiency (i.e., the fraction of baryons within halos that are converted into stars),  $f_{\text{gas}}(M_h)$  denotes the gas fraction retained inside a halo after photo-heating/photo-evaporation due to the rising ionizing UV background, and  $t_*(z) = c_* t_H(z)$  is the average star formation time scale, with  $t_H(z) = 1/H(z)$  being the local Hubble time and  $c_*$  a dimensionless constant. For halos that form within already ionized regions and are thus subject to radiative feedback, the gas fraction is modeled as  $f_{\text{gas}}(M_h) = 2^{-M_{\text{crit}}/M_h}$ , where  $M_{\text{crit}}$  denotes the characteristic halo mass capable of retaining 50% of its baryonic gas reservoir [121]. In contrast, for halos located in neutral regions where radiative feedback is absent, the gas fraction is assumed to be unity, i.e.,  $f_{\text{gas}}(M_h) = 1$ .

The monochromatic rest-frame UV luminosity ( $L_{\text{UV}}$ ) of a galaxy, which is derived from its star formation rate<sup>1</sup>, is likewise also modulated by the effects of radiative feedback during reionization. As a result, the relationship between halo mass and UV luminosity depends on whether a galaxy resides in an ionized or neutral region of the intergalactic medium. For galaxies that are unaffected by radiative feedback, their UV luminosity is determined as follows,

$$L_{\text{UV}}^{\text{nofb}}(M_h) = \frac{\dot{M}_*^{\text{nofb}}(M_h, z)}{\mathcal{K}_{\text{UV}}} = \frac{\varepsilon_{*,\text{UV}}(M_h, z)}{\mathcal{K}_{\text{UV},\text{fid}}} \left( \frac{\Omega_b}{\Omega_m} \right) M_h \quad (2.10)$$

Whereas in regions that have already been ionized, the associated UV background suppresses star formation in low-mass halos. The UV luminosity of galaxies in these feedback-affected regions is calculated as:

$$L_{\text{UV}}^{\text{fb}}(M_h) = 2^{-M_{\text{crit}}/M_h} L_{\text{UV}}^{\text{nofb}}(M_h) = 2^{-M_{\text{crit}}/M_h} \frac{\varepsilon_{*,\text{UV}}(M_h, z)}{\mathcal{K}_{\text{UV},\text{fid}}} \left( \frac{\Omega_b}{\Omega_m} \right) M_h \quad (2.11)$$

In these equations, the parameter  $\varepsilon_{*,\text{UV}}(M_h, z)$  denotes the UV efficiency of the halo and encapsulates several key parameters discussed above that govern star formation and the resulting ultraviolet emission in galaxies:

$$\varepsilon_{*,\text{UV}}(M_h, z) \equiv \frac{f_*(M_h, z)}{c_* t_H(z)} \frac{\mathcal{K}_{\text{UV},\text{fid}}}{\mathcal{K}_{\text{UV}}} \quad (2.12)$$

Assuming a star-formation efficiency parameterized as  $f_*(M_h) = f_{*,10} (M_h/10^{10} M_\odot)^{\alpha_*}$ , the UV efficiency parameter introduced in equation (2.12) takes the form -

$$\varepsilon_{*,\text{UV}}(M_h, z) = \frac{\varepsilon_{*,10,\text{UV}}}{t_H(z)} \left( \frac{M_h}{10^{10} M_\odot} \right)^{\alpha_*}, \quad (2.13)$$

where the normalization  $\varepsilon_{*,10,\text{UV}}$  is defined as :

$$\varepsilon_{*,10,\text{UV}} \equiv \frac{f_{*,10}}{c_*} \frac{\mathcal{K}_{\text{UV},\text{fid}}}{\mathcal{K}_{\text{UV}}}. \quad (2.14)$$

The rest-frame UV luminosities obtained from this model are finally converted to absolute UV magnitudes (in the AB system) using the relation [122, 123] -

$$\log_{10} \left( \frac{L_{\text{UV}}}{\text{ergs s}^{-1} \text{ Hz}^{-1}} \right) = 0.4 \times (51.6 - M_{\text{UV}}). \quad (2.15)$$

---

<sup>1</sup>The star formation rate and UV luminosity are related through the relation  $L_{\text{UV}} = \dot{M}_*(M_h, z)/\kappa_{\text{UV}}$ , wherein the constant conversion factor  $\kappa_{\text{UV}}$  is depends on the star formation history and characteristics of the stellar population, such as its age, metallicity, binarity, and the initial mass function (IMF).



Given a halo mass function and assuming each dark matter halo hosts only one galaxy, it is relatively straightforward to calculate the UV luminosity function using these  $M_h - L_{\text{UV}}$  relations mentioned above. The globally averaged UV luminosity function ( $\Phi_{\text{UV}}^{\text{total}}$ ) at a given redshift  $z$  is then obtained by appropriately combining the feedback-affected UV luminosity function ( $\Phi_{\text{UV}}^{\text{fb}}$ ) from ionized regions and the feedback-unaffected UV luminosity function ( $\Phi_{\text{UV}}^{\text{nofb}}$ ) from neutral regions, as follows -

$$\begin{aligned}\Phi_{\text{UV}}^{\text{total}}(z) &= Q_{\text{HII}}(z) \Phi_{\text{UV}}^{\text{fb}} + [1 - Q_{\text{HII}}(z)] \Phi_{\text{UV}}^{\text{nofb}} \\ &= Q_{\text{HII}}(z) \frac{dn}{dM_h} \left| \frac{dM_h}{dL_{\text{UV}}^{\text{fb}}} \right| \left| \frac{dL_{\text{UV}}^{\text{fb}}}{dM_{\text{UV}}} \right| + [1 - Q_{\text{HII}}(z)] \frac{dn}{dM_h} \left| \frac{dM_h}{dL_{\text{UV}}^{\text{nofb}}} \right| \left| \frac{dL_{\text{UV}}^{\text{nofb}}}{dM_{\text{UV}}} \right|, \quad (2.16)\end{aligned}$$

where  $Q_{\text{HII}}(z)$  is the globally averaged ionization fraction at redshift  $z$  and  $dn/dM_h$  is the dark matter halo mass function.

As evident from equation (2.16), the globally averaged ionized hydrogen fraction,  $Q_{\text{HII}}$ , constitutes a critical input for determining the UV luminosity function. In our model, we self-consistently follow the evolution of  $Q_{\text{HII}}$ , whose rate of change is controlled by the net balance between ionization and recombination processes in the intergalactic medium. For this calculation, the intrinsic ionizing photon production rate within a dark matter halo is modeled in terms of its star formation rate and the number of ionizing photons emitted per unit stellar mass formed ( $\eta_{\gamma*}$ ). However, not all ionizing photons produced within a halo can leak out and reach the intergalactic medium. We assume that the fraction of hydrogen ionizing photons that escapes into the intergalactic medium depends on the halo mass and is parameterized as  $f_{\text{esc}}(M_h) = f_{\text{esc},10} (M_h/10^{10} M_{\odot})^{\alpha_{\text{esc}}}$ .

Hence, the number density of ionizing photons per unit time contributed by feedback-unaffected galaxies is given by

$$\dot{n}_{\text{ion}}^{\text{nofb}}(z) = \eta_{\gamma*,\text{fid}} \int_{M_{\text{cool}}(z)}^{\infty} \varepsilon_{\text{esc}}(M'_h, z) \varepsilon_{*,\text{UV}}(M'_h, z) \left( \frac{\Omega_b}{\Omega_m} \right) M'_h \frac{dn}{dM_h}(M'_h, z) dM'_h \quad (2.17)$$

In contrast, the contribution from galaxies residing within ionized regions is regulated by radiative feedback and is computed as

$$\dot{n}_{\text{ion}}^{\text{fb}}(z) = \eta_{\gamma*,\text{fid}} \int_{M_{\text{cool}}(z)}^{\infty} 2^{-M_{\text{crit}}/M'_h} \varepsilon_{\text{esc}}(M'_h, z) \varepsilon_{*,\text{UV}}(M'_h, z) \left( \frac{\Omega_b}{\Omega_m} \right) M'_h \frac{dn}{dM_h}(M'_h, z) dM'_h \quad (2.18)$$

Here,  $M_{\text{cool}}(z)$  denotes the halo mass corresponding to the atomic cooling threshold (i.e.,  $T_{\text{vir}} = 10^4$  K) at redshift  $z$  and  $\varepsilon_{\text{esc}}(M_h, z)$  represents the escaping ionizing efficiency, defined as :

$$\varepsilon_{\text{esc}}(M_h, z) \equiv \frac{\mathcal{K}_{\text{UV}}}{\mathcal{K}_{\text{UV},\text{fid}}} \frac{\eta_{\gamma*}}{\eta_{\gamma*,\text{fid}}} f_{\text{esc}}(M_h, z) = \frac{\xi_{\text{ion}}}{\xi_{\text{ion},\text{fid}}} f_{\text{esc}}(M_h, z). \quad (2.19)$$

Given our assumption of  $f_{\text{esc}}(M_h)$  being a power-law function, the escaping ionizing efficiency can be written as

$$\varepsilon_{\text{esc}}(M_h, z) = \varepsilon_{\text{esc},10} \left( \frac{M_h}{10^{10} M_{\odot}} \right)^{\alpha_{\text{esc}}}, \quad (2.20)$$

where

$$\varepsilon_{\text{esc},10} \equiv \frac{\xi_{\text{ion}}}{\xi_{\text{ion},\text{fid}}} f_{\text{esc},10}. \quad (2.21)$$

The *total* comoving number density of ionizing photons that escapes into the intergalactic medium per unit time, and sources the growth of ionized regions, is therefore given by

$$\dot{n}_{\text{ion}}(z) = Q_{\text{HII}}(z) \dot{n}_{\text{ion}}^{\text{fb}}(z) + [1 - Q_{\text{HII}}(z)] \dot{n}_{\text{ion}}^{\text{nofb}}(z) \quad (2.22)$$

We adopt a fiducial value of  $\mathcal{K}_{\text{UV},\text{fid}} = 1.15485 \times 10^{-28} \text{M}_{\odot} \text{yr}^{-1} / \text{ergss}^{-1} \text{Hz}^{-1}$  and  $\eta_{\gamma*,\text{fid}} = 4.62175 \times 10^{60}$  photons per  $\text{M}_{\odot}$  in all our calculations. These values were obtained using STARBURST99 v7.0.1<sup>2</sup>[124] for a stellar population with a Salpeter IMF (0.1 - 100  $\text{M}_{\odot}$ ) and metallicity  $Z = 0.001 (= 0.05 Z_{\odot})$  at an age of 100 Myr, assuming continuous star formation. The assumed fiducial values for  $\mathcal{K}_{\text{UV}}$  and  $\eta_{\gamma*}$  correspond to an ionizing photon production efficiency  $\log_{10} [\xi_{\text{ion},\text{fid}} / (\text{ergs}^{-1} \text{Hz})] \approx 25.23$ , which is consistent with the latest measurements from JWST [125–127].

Once the global reionization history  $Q_{\text{HII}}(z)$  is obtained, the Thomson scattering optical depth of the CMB photons for that particular model can be computed as

$$\tau_{\text{el}} \equiv \tau(z_{\text{LSS}}) = \sigma_T \bar{n}_H c \int_0^{z_{\text{LSS}}} \frac{dz'}{H(z')} (1 + z')^2 \chi_{\text{He}}(z') Q_{\text{HII}}(z'), \quad (2.23)$$

where  $z_{\text{LSS}}$  is the redshift of last scattering,  $\bar{n}_H$  is the current mean comoving number density of hydrogen, and  $\sigma_T$  is the Thomson scattering cross-section.

Before proceeding ahead, we note that our theoretical model includes **five** free parameters that describe the astrophysical properties of high-redshift galaxies - namely,  $\log_{10}(\varepsilon_{*,10,\text{UV}})$ ,  $\alpha_*$ ,  $\log_{10}(\varepsilon_{\text{esc},10})$ ,  $\alpha_{\text{esc}}$ , and  $\log_{10}(M_{\text{crit}}/M_{\odot})$ .

### 3 Observational Datasets and Likelihood Analysis

We compare the theoretical predictions of the model described in the previous section with several available observational datasets. In this section, we briefly summarize them and also describe the Bayesian formalism used to constrain the free parameters of our model.

1. **Thomson scattering optical depth of CMB photons:** Throughout this work (except in Section 4.2), we use the latest measurement of  $\tau_{\text{el}} = 0.0540 \pm 0.0074$  reported by the Planck collaboration [6].
2. **Global Reionization History:** We utilize estimates of the globally averaged fraction of intergalactic neutral hydrogen ( $Q_{\text{HI}} = 1 - Q_{\text{HII}}$ ) at different redshifts derived from Lyman- $\alpha$  absorption studies of distant quasars and galaxies, similar to our previous work [48, 49].
3. **Galaxy UV Luminosity Functions:** We make use of observational data for the galaxy UV luminosity function,  $\Phi_{\text{UV}}(M_{\text{UV}}, z)$ , compiled across nine redshifts in the range  $5 \leq z < 14$ . These measurements are obtained from a combination of surveys carried out with the Hubble Space Telescope [128] and the James Webb Space Telescope [33–36, 129].

Following our previous work, we consider only the observational data points with  $M_{\text{UV}} \geq -21$  from these studies in our analysis [130] since our theoretical model does not incorporate the effects of feedback from active galactic nuclei (AGN) activity or the significant dust attenuation present in bright galaxies.

---

<sup>2</sup><https://www.stsci.edu/science/starburst99/docs/default.htm>

We adopt a Bayesian framework to constrain the free parameters of our model by comparing its predictions against the set of observational constraints discussed above. In this approach, we compute the posterior probability distribution,  $\mathcal{P}(\boldsymbol{\theta}|\mathcal{D})$ , of the model parameters  $\boldsymbol{\theta}$  given the data  $\mathcal{D}$ , using Bayes' theorem:

$$\mathcal{P}(\boldsymbol{\theta}|\mathcal{D}) = \frac{\mathcal{L}(\mathcal{D}|\boldsymbol{\theta})\pi(\boldsymbol{\theta})}{\mathcal{Z}}, \quad (3.1)$$

where  $\mathcal{L}(\mathcal{D}|\boldsymbol{\theta})$  is the likelihood function, representing the conditional probability distribution of the data  $\mathcal{D}$  given the model parameters  $\boldsymbol{\theta}$ ;  $\pi(\boldsymbol{\theta})$  is the prior distribution of the model parameters; and  $\mathcal{Z} = \int \mathcal{L}(\mathcal{D}|\boldsymbol{\theta}) \pi(\boldsymbol{\theta}) d\boldsymbol{\theta}$  is the Bayesian evidence. Since our focus is on parameter estimation rather than model comparison, the evidence  $\mathcal{Z}$  serves only as a normalization constant and does not play any role in our analysis.

Assuming the different observational datasets to be statistically independent, the joint total likelihood is calculated as the product of the individual likelihoods:

$$\mathcal{L}(\mathcal{D}|\boldsymbol{\theta}) = \prod_{\alpha} \mathcal{L}(\mathcal{D}_{\alpha}|\boldsymbol{\theta}), \quad (3.2)$$

where  $\alpha$  indexes the individual datasets included in the analysis. The likelihood for a particular dataset  $\mathcal{D}_{\alpha}$  is given by

$$\mathcal{L}(\mathcal{D}_{\alpha}|\boldsymbol{\theta}) = \exp \left[ -\frac{1}{2} \chi^2(\mathcal{D}_{\alpha}, \boldsymbol{\theta}) \right] = \exp \left[ -\frac{1}{2} \sum_i \left( \frac{\mathcal{D}_{\alpha,i} - \mathcal{M}_{\alpha,i}(\boldsymbol{\theta})}{\sigma_{\alpha,i}} \right)^2 \right], \quad (3.3)$$

where  $\mathcal{D}_{\alpha,i}$  and  $\sigma_{\alpha,i}$  are the observed value and its associated uncertainty for the  $i$ -th data point, respectively, and  $\mathcal{M}_{\alpha,i}(\boldsymbol{\theta})$  is the model prediction corresponding to that data point.

In order to facilitate a fair comparison between the predictions from our  $\text{CPL}n\Lambda\text{CDM}$  models and the observed galaxy UV luminosities and number densities reported in these studies, originally derived from the flux and number counts respectively under the assumption of a specific cosmological model (viz.,  $\Lambda\text{CDM}$ ), we need to make relevant corrections that would convert it to what they would be if interpreted by an observer assuming a  $\Lambda\text{CDM}$  cosmology. The ‘‘corrected’’ UV luminosity function  $\Phi'_{\text{UV}}$  and UV magnitude  $M'_{\text{UV}}$  are given by,

$$\Phi'_{\text{UV}} = \Phi_{\text{UV}} \times \frac{(dV/dz)_{\text{CPL}n\Lambda\text{CDM}}}{(dV/dz)_{\Lambda\text{CDM}}}, \quad (3.4)$$

$$M'_{\text{UV}} = M_{\text{UV}} - 2.5 \log_{10} \left[ \left( \frac{D_{\text{L}}^{\Lambda\text{CDM}}}{D_{\text{L}}^{\text{CPL}n\Lambda\text{CDM}}} \right)^2 \right], \quad (3.5)$$

where  $dV/dz$  and  $D_{\text{L}}$  are the differential comoving volume and luminosity distance at the redshift of interest.

Throughout this paper, all galaxy number densities and UV luminosities shown in figures and discussed in the text for the  $\text{CPL}n\Lambda\text{CDM}$  model will refer to these corrected quantities.

Another important caveat in our analysis involves the treatment of the neutral hydrogen fraction ( $Q_{\text{HI}}$ ) measurements obtained by various studies referenced in point 2 above. We assume that these constraints are primarily sensitive to the astrophysical modeling rather than the underlying cosmological model (viz.,  $\Lambda\text{CDM}$ ). Since reinterpreting these  $Q_{\text{HI}}$  measurements within a different cosmological framework is non-trivial, we adopt the published values without modification in our likelihood calculations for the  $\text{CPL}n\Lambda\text{CDM}$  models to keep the analysis simple.

**Table 1:** Constraints on the *astrophysical* free parameters of the  $\text{CPL}n\Lambda\text{CDM}$  model from the MCMC-based analysis. The parameters are assumed to follow uniform priors within the ranges specified in the second column. The numbers in the other columns show the mean value with  $1\sigma$  errors for these parameters, as obtained for the two cases described in Section 4.1 and Section 4.2 respectively. Note that  $\tau_{\text{el}}$  is a derived parameter in our analysis.

Parameters	Priors	fiducial $\text{CPL}n\Lambda\text{CDM}$	maxboost $\text{CPL}n\Lambda\text{CDM}$
$\log_{10} (\varepsilon_{*10,\text{UV}})$	$[-3.0, 0.5]$	$-1.224 \pm 0.033$	$-0.813^{+0.032}_{-0.028}$
$\alpha_*$	$[-1.0, 1.0]$	$0.338 \pm 0.031$	$0.228^{+0.026}_{-0.029}$
$\log_{10} (\varepsilon_{\text{esc},10})$	$[-3.0, 1.0]$	$-0.822 \pm 0.047$	$-0.841 \pm 0.028$
$\alpha_{\text{esc}}$	$[-3.0, 1.0]$	$-0.23 \pm 0.12$	$-0.087^{+0.063}_{-0.072}$
$\log_{10}(M_{\text{crit}}/M_{\odot})$	$[9.0, 11.0]$	$< 9.62$	$10.496^{+0.096}_{-0.081}$
$\tau_{\text{el}}$	-	$0.0548^{+0.0029}_{-0.0032}$	$0.0597^{+0.0028}_{-0.0031}$

## 4 Results and Discussion

### 4.1 A fiducial model: success with JWST, tension with the CMB

In our earlier works, we explained the high-redshift observations discussed in Section 3 by invoking a redshift evolution in the astrophysical parameters governing galaxy formation and evolution, while assuming a  $\Lambda\text{CDM}$  background cosmology. For completeness, we summarize the constraints obtained from such an analysis in Appendix A using the  **$\Lambda\text{CDM}$  (Planck 2018)** cosmological parameters.

However, in this work, our aim is to assess the viability of cosmological models beyond  $\Lambda\text{CDM}$  in explaining these high-redshift datasets, *without invoking any evolution in the astrophysical properties of early galaxies*. For this purpose, we choose a fiducial model in the  $\text{CPL}n\Lambda\text{CDM}$  cosmology, whose dark energy sector is characterized by the parameters -  $\Omega_{\Lambda} = -1, w_0 = -1.05, w_a = 0.7$ . As has been the recent practice in literature [105, 110, 131, 132], we fix all other relevant cosmological parameters — such as  $H_0, \Omega_m, \sigma_8$ , and  $n_s$  — to their  **$\Lambda\text{CDM}$  (Planck 2018)** best-fit values, as described at the end of Section 1, while noting that this approach ignores potential correlations between cosmological parameters. From Figures 1 and 2, we have already seen that the number density of dark matter halos at  $z > 10$  in this **fiducial  $\text{CPL}n\Lambda\text{CDM}$**  cosmology is significantly larger than in the  $\Lambda\text{CDM}$  cosmology.

We therefore perform a Markov chain Monte Carlo (MCMC) analysis to constrain the *astrophysical* parameters for this cosmological model by comparing its theoretical predictions

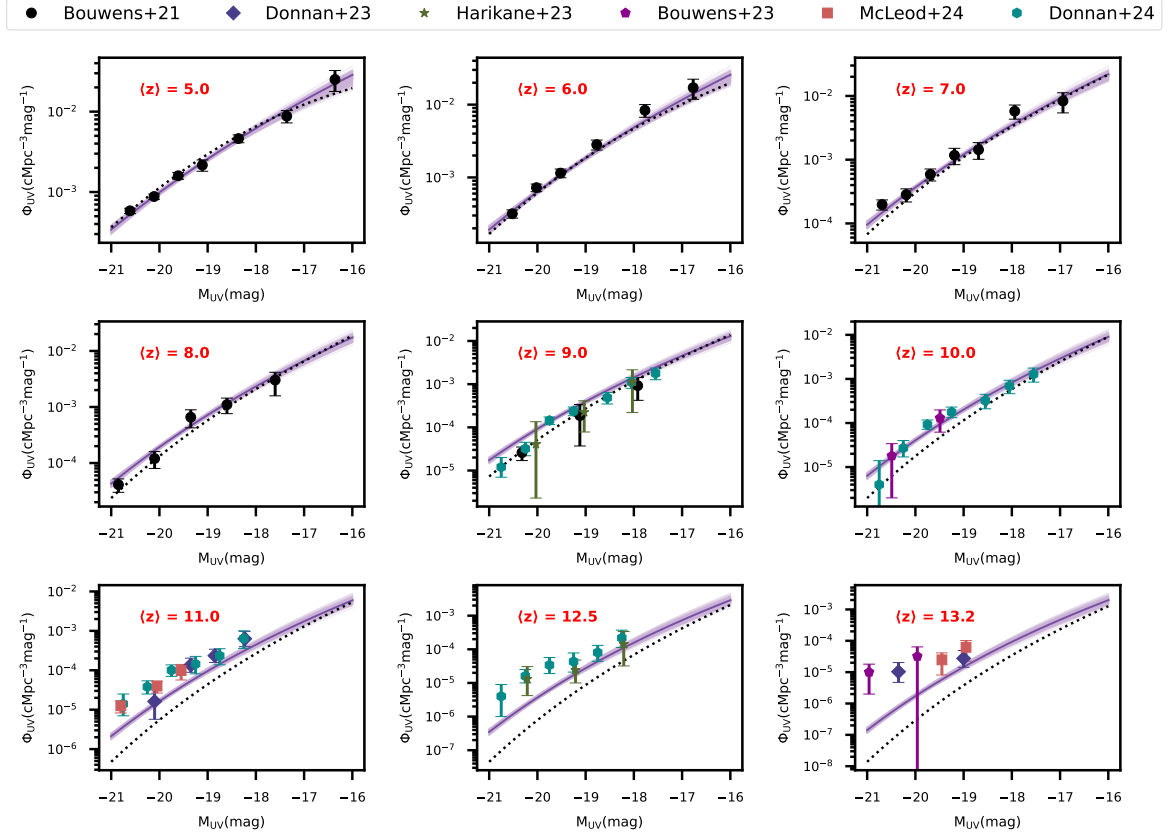


**Figure 3:** The galaxy UV luminosity functions at nine different redshifts (with their respective mean values  $\langle z \rangle$  mentioned in the upper left corner) for 200 random samples drawn from the MCMC chains of the **fiducial CPLn $\Lambda$ CDM** case. In each panel, the solid dark-violet line corresponds to the best-fit model, while the colored data points show the different observational constraints [33–36, 128, 129] used in the likelihood analysis. The prediction from a model within the  $\Lambda$ CDM (**Planck 2018**) cosmology that best matches the observational measurements at  $z < 10$  and does not assume any evolution in the UV efficiency parameters above  $z \sim 10$  is also shown using black dotted lines.

with the various observations listed in the previous section. We shall henceforth refer to this case as the “**fiducial CPLn $\Lambda$ CDM**” model. The marginalized constraints on the free parameters are mentioned in the first column of Table 1. We show the model-predicted UVLFs for 200 random samples from the MCMC chains in Figure 3, and their corresponding reionization histories in Figure 4.

A natural consequence of a larger abundance of halos at higher redshifts in the **fiducial CPLn $\Lambda$ CDM** cosmological model compared to  $\Lambda$ CDM is an increased number density of massive UV-luminous galaxies at high redshifts, particularly at  $z > 10$ . As a result, this model shows noticeably better agreement with the UVLF observations at  $z > 10$  than the predictions from the  $\Lambda$ CDM model at these redshifts under the assumption of a redshift-independent UV production efficiency (shown as black dotted lines in Figure 3). We find that reproducing the observed UVLFs over the redshift range  $5 \leq z < 14$  in this cosmological framework requires a relatively lower UV efficiency in galaxies on average ( $\varepsilon_{*10,UV} \approx 0.05$ )

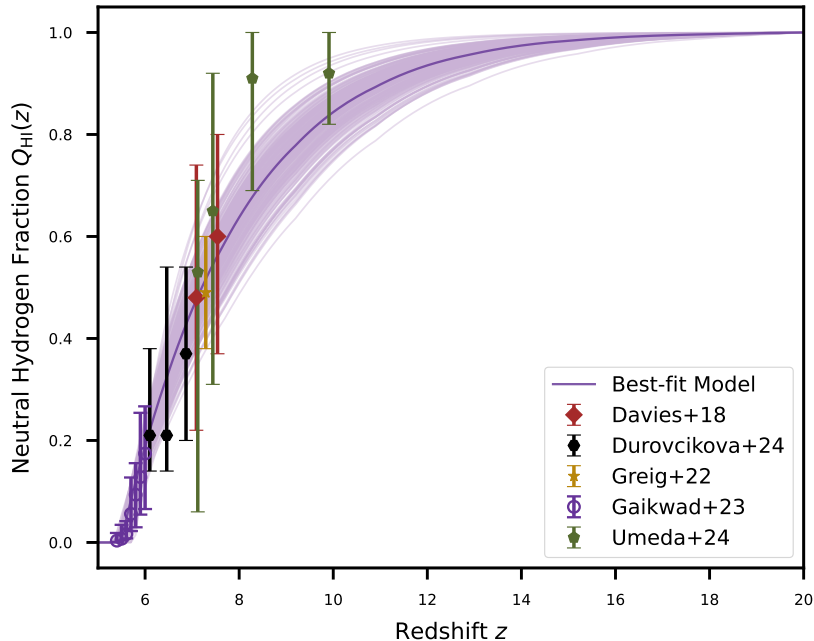


**Figure 4:** The evolution of the globally averaged intergalactic neutral hydrogen fraction as a function of redshift for 200 random samples drawn from the MCMC chains of the **fiducial CPLnΛCDM** case. The colored data points represent the observational measurements of  $Q_{\text{HI}}(z)$  used in the analysis.

compared to that required in  $\Lambda$ CDM cosmology, where  $\varepsilon_{*10,\text{UV}} \approx 0.13$  at  $z \lesssim 9$  and increases further at higher redshifts (see Appendix A). However, as shown in Figure 3, the **fiducial CPLnΛCDM** model still falls short in reproducing the full shape of the observed UVLFs at  $z \geq 11$ , particularly at the bright end. This suggests that introducing a modest redshift evolution in the astrophysical parameters—potentially in the slope of the halo mass–stellar mass relation ( $\alpha_*$ )— may be essential for bringing the UVLF predictions of the **fiducial CPLnΛCDM** cosmological model into better agreement with the observations.

As seen in Figure 4, the **fiducial CPLnΛCDM** model is also able to satisfy the various observational constraints on the progress of reionization. We obtain an escaping ionizing efficiency of  $\approx 15\%$  for  $10^{10} M_\odot$  halos and find  $\varepsilon_{\text{esc}}$  to be negatively correlated with halo mass, similar to the trends obtained for reionization-era galaxies within the  $\Lambda$ CDM cosmological model (Table 3).

While the analysis thus far may seem very promising and motivate a comprehensive MCMC study involving the simultaneous variation of both cosmological and astrophysical parameters to find models in CPLnΛCDM cosmology that explain these high- $z$  galaxy observations, we pause to assess the broader viability of the **fiducial CPLnΛCDM** model beyond the high-redshift UVLFs and reionization datasets considered above — particularly in light of the wealth of high-precision cosmological observations that tightly constrain the evolutionary history of our Universe.

The temperature and polarization anisotropies observed in the CMB provide one of the most stringent tests of any cosmological model, as they encode detailed information about the Universe’s expansion history, composition, and geometry. The oscillatory features imprinted in the CMB power spectra define a characteristic angular scale  $\theta_*$  on the sky, which is given

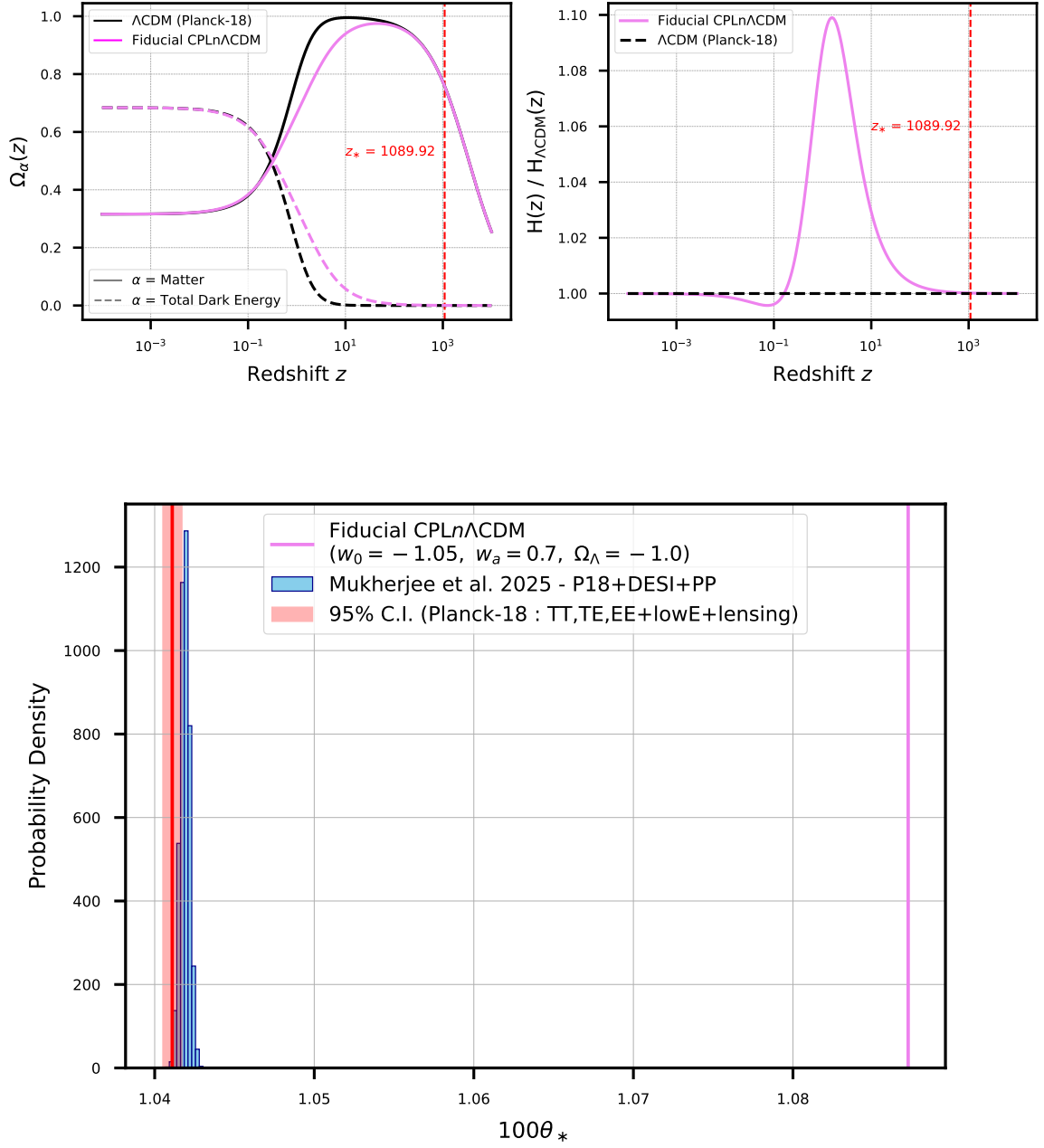


**Figure 5:**

**Top:** Comparison of the evolution of energy densities and expansion rates across different cosmological models. The left panel shows the redshift evolution of the matter density (solid lines) and the total dark energy density (dashed lines). The right panel presents the ratio of the Hubble parameter in our fiducial CPLn $\Lambda$ CDM model to that in the  $\Lambda$ CDM model, as a function of redshift.

**Bottom:** The angular acoustic scale  $\theta_*$  corresponding to acoustic oscillations imprinted in the CMB power spectra. The solid violet line indicates the value of  $100\theta_*$  predicted by the **fiducial CPLn $\Lambda$ CDM** model (see Section 4.1), while the red shaded region represents the corresponding 95% confidence interval derived from the Planck-2018 analysis. The histogram in blue shows the distribution of  $100\theta_*$  for all CPLn $\Lambda$ CDM models, that are consistent with other cosmological data such as CMB, BAO, SNe-Ia (Section 4.2), taken from the MCMC chains of Mukherjee et al. (2025).



by  $\theta_* = r_*/D_M(z_*)$  where  $r_*$  is the comoving sound horizon at recombination and  $D_M(z_*)$  is the comoving angular diameter distance to the recombination epoch at a redshift of  $z_*$ . This angular acoustic scale has been measured to an extremely high precision (0.03%) by the latest Planck observations and is only weakly dependent on the cosmological model.

We present the evolution of the energy densities of the individual components, along with the Hubble expansion rate, for the **fiducial CPLn $\Lambda$ CDM** cosmological model in the top panel of Figure 5. Notably, both quantities converge to their  $\Lambda$ CDM counterparts prior to the epoch of recombination. Given that the size of the sound horizon at recombination  $r_*$  is primarily determined by the speed of sound in the photon-baryon fluid, which in turn depends on the baryon-to-photon density ratio, and the pre-recombination expansion history, we can therefore safely assume that its value remains unchanged in the **fiducial CPLn $\Lambda$ CDM** model. It is then straightforward to calculate  $D_M(z_*)$  and thereafter, the value of  $\theta_*$  for the cosmological model under consideration. However, as shown in the bottom panel of Figure 5, the angular acoustic scale ( $100\theta_*$ ) corresponding to the **fiducial CPLn $\Lambda$ CDM** model is considerably larger than not only the constraints obtained from the Planck-2018  $\Lambda$ CDM analysis but also those corresponding to the class of CPLn $\Lambda$ CDM models that provide good fits to a wide range of other cosmological observations, including the CMB power spectra. This indicates that while the **fiducial CPLn $\Lambda$ CDM** model shows promise by exhibiting better agreement with the high-redshift UVLF observations from JWST than our baseline  **$\Lambda$ CDM (Planck 2018)** model, it is in strong tension with, and effectively ruled out by, other cosmological datasets—in this case, the CMB itself. This highlights the importance of exercising caution when interpreting apparent successes of cosmological models in explaining isolated datasets.

As a result, we now extend our analysis by incorporating constraints from other standard cosmological probes, in order to identify more viable regions of parameter space within the CPLn $\Lambda$ CDM cosmological framework.

#### 4.2 A viable CPLn $\Lambda$ CDM model exhibiting maximum boost in halo abundance (relative to $\Lambda$ CDM) at high redshifts ( $z \approx 13.2$ )

Recently, Mukherjee et al. (2025) [108] carried out a comprehensive MCMC-based exploration of CPLn $\Lambda$ CDM models that are compatible with a variety of cosmological observations—including CMB temperature, polarization, and lensing measurements from the Planck mission [6], baryon acoustic oscillations (BAO) data obtained by the Dark Energy Spectroscopic Instrument (DESI) Collaboration [133], and the Pantheon-Plus compilation of Type Ia supernovae light curves [134]. We summarize the constraints obtained on the cosmological parameters from their analysis in Appendix B.

**Table 2:** Cosmological parameters for the CPLn $\Lambda$ CDM model that remains consistent with other cosmological observations while yielding the maximum enhancement in the abundance of dark matter halos at  $z = 13.2$ , relative to the baseline  **$\Lambda$ CDM (Planck 2018)** cosmological model.

$\Omega_m$	$\Omega_b h^2$	$\Omega_\Lambda$	$h$	$\Omega_\phi$
0.31012	0.0223509	-0.117409	0.682049	0.807211
$w_0$	$w_a$	$n_s$	$\sigma_8$	$\tau_{\text{el}}$
-0.887089	-0.623657	0.966626	0.847624	0.0699301

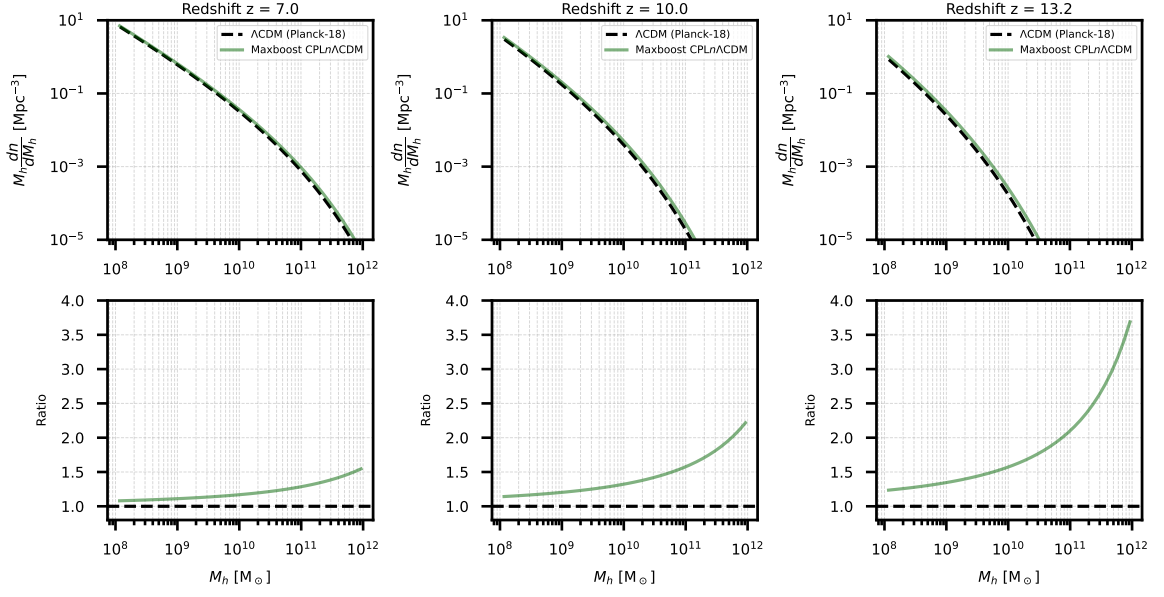


**Figure 6:** Comparison of the dark matter halo mass functions at high redshifts ( $z = 7, 10$ , and  $13.2$ ) for the **maxboost**  $\text{CPLn}\Lambda\text{CDM}$  and the baseline  $\Lambda\text{CDM}$  (Planck 2018) cosmological models.

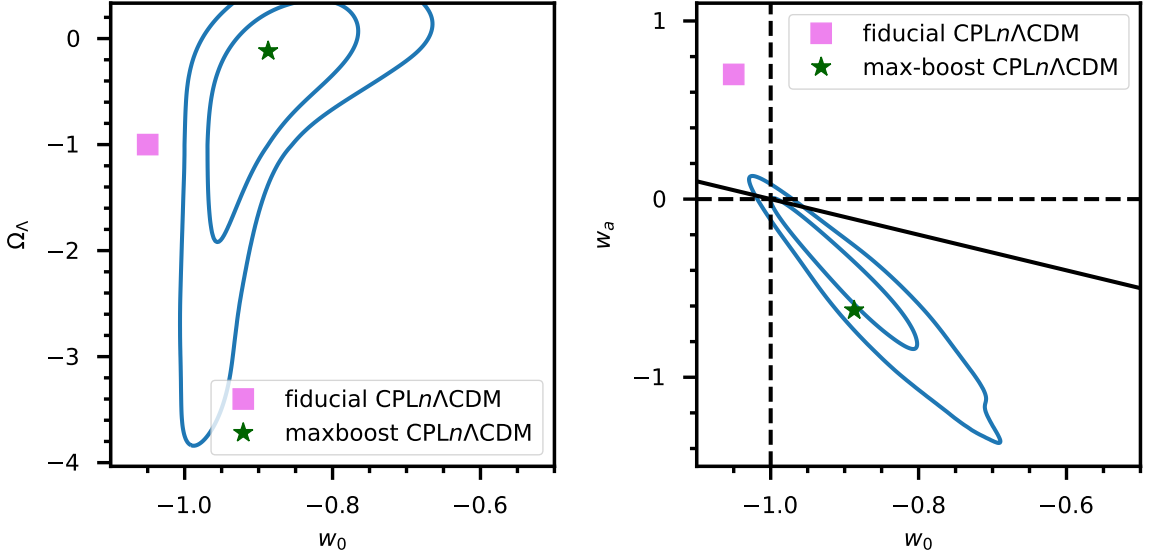


**Figure 7:** The two-dimensional joint posterior distributions for some pairs of free parameters in the  $\text{CPLn}\Lambda\text{CDM}$  model obtained in Mukherjee et al. (2025) by comparing against the Planck-2018 CMB temperature, polarization, and lensing datasets, the DESI BAO measurements, and Pantheon-Plus compilation of Type-Ia supernovae light curves. The blue solid contours are drawn at 68% and 95% confidence levels. In each panel, the **fiducial**  $\text{CPLn}\Lambda\text{CDM}$  and the **maxboost**  $\text{CPLn}\Lambda\text{CDM}$  models are denoted using a violet square and a green star symbol, respectively.

Instead of undertaking a complete exploration of the combined cosmological and astrophysical parameter space within the  $\text{CPLn}\Lambda\text{CDM}$  framework, we make use of samples from the posterior chains of Mukherjee et al. (2025) that are already consistent with several key cosmological datasets. This is sufficient to investigate the prospects of the “allowed”  $\text{CPLn}\Lambda\text{CDM}$  models in explaining the high-redshift galaxy and reionization observations. For our analysis in this subsection, we discard the initial 30% of the steps from their chains as burn-in and utilize the remaining samples.

From their chains, we identify the  $\text{CPLn}\Lambda\text{CDM}$  model that gives the maximum enhancement in the abundance of dark matter halos at  $z \approx 13.2$ , relative to the baseline  $\Lambda\text{CDM}$  (Planck 2018) cosmological model. We shall refer to this as the “**maxboost CPLn** $\Lambda\text{CDM}$ ” model, whose corresponding cosmological parameters are listed in Table 2. As seen in Figure 6, this model yields a modest enhancement in halo number densities compared to the  $\Lambda\text{CDM}$  model — approximately a factor of 2 for  $10^{11}M_\odot$  halos at  $z = 13.2$ . We show this particular model within the marginalized two-dimensional space of some parameter combinations in Figure 7. As noted in the previous section, it is not surprising that the **fiducial CPLn** $\Lambda\text{CDM}$  model (indicated by violet square symbols) lies outside the 95% confidence region and is therefore ruled out at high significance.

As before, we perform an MCMC analysis to constrain the *astrophysical* parameters of this model, under the assumption that they *do not evolve with redshift*. For the likelihood calculations, we take the reionization optical depth corresponding to this model ( $\tau_{\text{el}} = 0.0699301$ , listed in Table 2) as the observational estimate. Its associated uncertainty is assumed to be the same as that obtained from the full MCMC chains (see Appendix B), namely,  $\Delta\tau_{\text{el}} = 0.0073$ .

The marginalized constraints on the free parameters are presented in the second column of Table 1. We show the model-predicted UVLFs for 200 random samples from the MCMC chains in Figure 8, and their corresponding reionization histories in Figure 9. We find that the UVLFs predicted by the **maxboost CPLn** $\Lambda\text{CDM}$  model are only marginally enhanced compared to those from the  $\Lambda\text{CDM}$  model. The predicted UVLFs are comparatively lower than the observational measurements of the bright-end ( $M_{\text{UV}} \leq -20$ ) at  $z \gtrsim 11$ , with the discrepancy growing increasingly severe at higher redshifts. By  $z \approx 13$ , the predicted UVLF is consistently lower than the observed data across the entire range of UV magnitudes probed by observations. The model is, however, consistent with constraints on the progress of reionization as shown in Figure 9. As seen from Figures 9 and 10, reionization in the **maxboost CPLn** $\Lambda\text{CDM}$  model is more extended and starts earlier compared to the baseline  $\Lambda\text{CDM}$  (Planck 2018) cosmological model, yielding a larger value of  $\tau_{\text{el}}$ . However, the mean electron scattering optical depth derived from the MCMC chains ( $\tau_{\text{el}} \approx 0.0597$ ) is  $\approx 1.3\sigma$ <sup>3</sup> lower than the value ( $\tau_{\text{el}} \approx 0.0699$ ) corresponding to this cosmological model. This may be attributed to the inclusion of  $Q_{\text{HI}}$  measurements (without any correction, from the different studies) in the likelihood calculation, which prevents reionization histories with arbitrarily large values of  $\tau_{\text{el}}$  from being accepted while scanning the parameter space. The escaping ionizing efficiency exhibits a weak dependence on halo mass, characterized by a marginally negative power-law slope of  $\alpha_{\text{esc}} = -0.087_{-0.072}^{+0.063}$ . Interestingly, the critical halo mass  $M_{\text{crit}}$  affected by radiative feedback is found to be approximately  $10^{10.5}M_\odot$ , which is slightly higher than that obtained within the baseline  $\Lambda\text{CDM}$  (Planck 2018) model (Appendix A). This higher threshold not only facilitates the completion of reionization by  $z \approx 5$ , but also enables

<sup>3</sup>Here, the  $\sigma$  has been estimated using the quadrature sum of the two individual ‘symmetrized’ error uncertainties

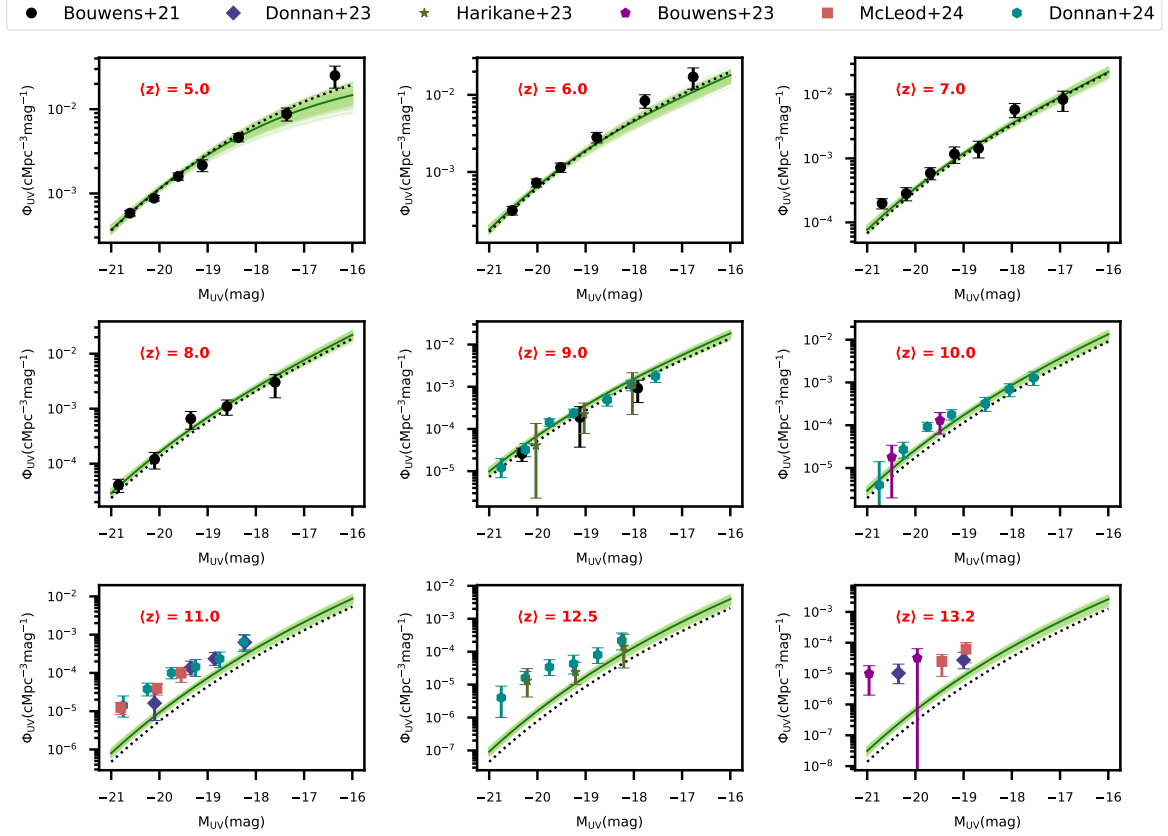


**Figure 8:** The galaxy UV luminosity functions at nine different redshifts (with their respective mean values  $\langle z \rangle$  mentioned in the upper left corner) for 200 random samples drawn from the MCMC chains of the **maxboost CPLn $\Lambda$ CDM** model. In each panel, the solid dark-green line corresponds to the best-fit model, while the colored data points show the different observational constraints [33–36, 128, 129] used in the likelihood analysis. The prediction from a model within the baseline  $\Lambda$ CDM (**Planck 2018**) cosmology that best matches the observational measurements at  $z < 10$  and does not assume any evolution in the UV efficiency parameters above  $z \sim 10$  is also shown using black dotted lines.

the model to remain consistent with the observed UVLFs at lower redshifts ( $z < 7$ , when radiative feedback is dominant with reionization nearing completion) so that the redshift-independent UV efficiency parameter,  $\varepsilon_{*10,UV}$ , can be flexibly calibrated to reproduce the UVLF observations across the entire redshift range of  $5 \leq z < 14$ .

Therefore, our analysis reveals that the **maxboost CPLn $\Lambda$ CDM** cosmological model struggles to simultaneously reproduce the full shape and evolution of the UVLFs across the redshift range  $5 \leq z < 14$ , when assuming redshift-independent astrophysical properties for high- $z$  galaxies. Our findings lend support to the growing consensus in recent literature that cosmological modifications *alone* are likely insufficient to account for the unexpectedly high abundance of  $z > 10$  galaxies observed by JWST. For instance, Sabti et al. (2024) [82] recently concluded that alterations to the  $\Lambda$ CDM matter power spectrum (and thereby, leading to an enhancement of the halo mass function) that is large enough to reproduce the abundance of  $z > 10$  JWST candidates would lead to inconsistencies with the UVLFs

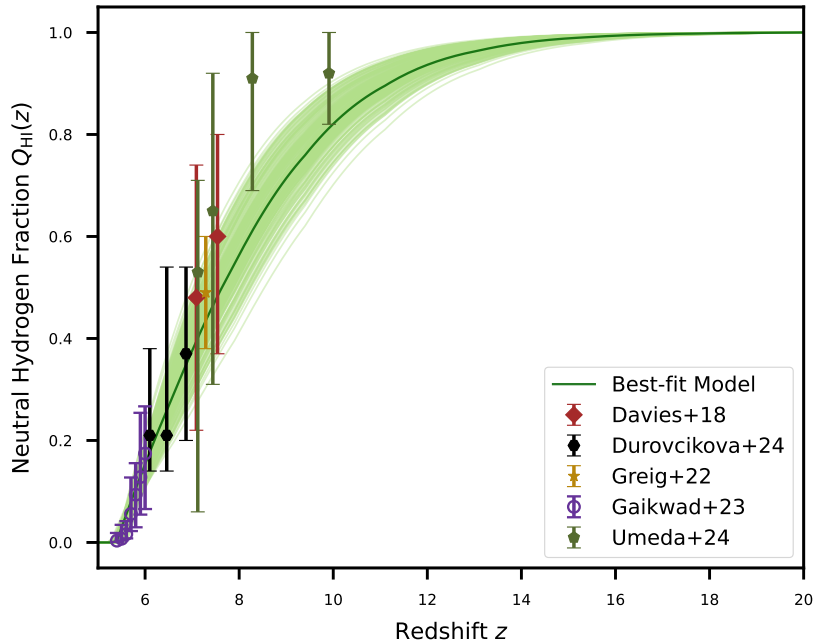


**Figure 9:** The evolution of the globally averaged intergalactic neutral hydrogen fraction as a function of redshift for 200 random samples drawn from the MCMC chains of the **maxboost CPLn $\Lambda$ CDM** model. The colored data points indicate the observational measurements of  $Q_{\text{HI}}(z)$  used in the analysis.

measured by HST at lower redshifts and/or other cosmological datasets. Similarly, Shen et al. (2024) [70] showed that while cosmological models incorporating early dark energy (EDE) can successfully reproduce the UVLFs in the range  $4 \lesssim z \lesssim 10$ , they still require either a modest increase in star formation efficiency or a nominal degree of stochasticity in UV emission from galaxies to match the JWST observations at higher redshifts -  $12 \lesssim z \lesssim 16$ . A similar issue was also noted by Liu et al. (2024) [71] while investigating the prospects of explaining the JWST observations using EDE models, where they found that these models can match the UVLFs at  $z > 10$  better than  $\Lambda$ CDM but don't fare well as well as  $\Lambda$ CDM at lower redshifts ( $z < 10$ ).

Given that even the CPLn $\Lambda$ CDM model with maximal halo abundance at  $z \approx 13$  fails to consistently reproduce the observed evolution of the UV luminosity function from  $z = 13.2$  to  $z = 5$ , we also check whether a model that maximizes the ratio of the boost in halo abundances (relative to the baseline  $\Lambda$ CDM (**Planck 2018**) model) between  $z = 13.2$  and  $z = 5$  can provide a better match (see Appendix C for details). We find that the results remain unchanged, underscoring the difficulty CPLn $\Lambda$ CDM cosmological models face in simultaneously reproducing the galaxy UV luminosity function across the full redshift range from  $z = 13.2$  to  $z = 5$ , without any astrophysical evolution.

We should mention here that several intriguing proposals have been explored in the literature that argue in favor of cosmological solutions for the JWST galaxy excess. For instance, Padmanabhan & Loeb (2023) investigated how a modified matter transfer function could enhance early structure formation [81], while Menci et al. (2024) examined models incorporating a negative cosmological constant, similar in spirit to the framework we use here [110]. Our analysis is intended to build upon this line of inquiry by focusing on a specific and

crucial question: to what extent can such models enhance the early halo abundance while remaining simultaneously consistent with the full suite of precision cosmological datasets (e.g., CMB, BAO, SNe)? This focus is motivated by our finding in this section that some promising high-redshift models can face challenges when confronted with these other stringent constraints. By carefully selecting for CPLn $\Lambda$ CDM models that satisfy this holistic viability, our work quantifies the level of enhancement permitted by the existing cosmological data. Our finding that even these models fall short of fully explaining the observations strengthens the case that modifications to astrophysics are a key part of the complete solution.

## 5 Conclusion

The James Webb Space Telescope (JWST) is revolutionizing our view of the early universe by revealing an unexpected abundance of luminous galaxies at redshifts  $z > 10$  [21–41]. The existence of these ultra-luminous galaxies at very early cosmic epochs challenges the standard cosmological model,  $\Lambda$ CDM, prompting a critical re-evaluation of the intertwined physics of cosmic expansion and early galaxy formation. This work confronts a key question: Can modifications to cosmology *alone* account for these surprising observations, or are changes to our understanding of galaxy formation physics inevitable?

We investigate a promising class of alternative models featuring dynamical dark energy and a negative cosmological constant (CPLn $\Lambda$ CDM). Using a self-consistent framework that couples galaxy evolution with cosmic reionization [48, 49], we test whether such a model, itself constrained by established cosmological data like the CMB, can reproduce the observed galaxy populations from  $z \approx 5$  to  $z \approx 14$  *without invoking any evolution in their astrophysical properties*. Our principal conclusions are:

- **A purely cosmological enhancement is insufficient.** While CPLn $\Lambda$ CDM models that are consistent with other cosmological probes perform slightly better than the standard  $\Lambda$ CDM scenario at  $z > 10$ , they fail to reproduce the full shape and evolution of the observed galaxy UV luminosity function across the redshift range  $5 \leq z < 14$ . They cannot, on their own, resolve the tension. This suggests that some degree of evolution in the astrophysical properties of high-redshift galaxies — albeit less pronounced — may still be necessary.
- **High-redshift observations must be reconciled with the established cosmic history.** Our analysis serves as a crucial case study, demonstrating that any proposed cosmological solution to the early galaxy excess must be rigorously tested against the full suite of precision cosmological observations. Apparent successes in one observational regime can be decisively ruled out by constraints from another.

Our findings contribute to a growing consensus that the surprising abundance of early, bright galaxies is unlikely to be resolved by modifications to the cosmological model alone [82, 83] and that even under modified cosmological scenarios, an evolution in galaxy properties is still required [70, 71]. This places renewed emphasis on understanding the astrophysical processes, such as star formation efficiency, feedback, or a top-heavy stellar initial mass function, that govern galaxy formation in the first billion years. Assuming plausible ionizing properties for high-redshift galaxies, CPLn $\Lambda$ CDM models also produce a reionization history consistent with constraints on the ionization state of the intergalactic medium derived from



astrophysical observations. We note, however, that these constraints have not been explicitly evaluated for alternative cosmologies such as the one considered here.

Perhaps more importantly, this work demonstrates a powerful synergy. We show that the available datasets of high-redshift galaxies are not only probes of astrophysics but can also serve as a potent new tool to constrain fundamental cosmology. By systematically marginalizing over uncertain galaxy properties, we turn the challenge posed by JWST into a novel opportunity to test the viability of beyond- $\Lambda$ CDM models.

A crucial next step is to move beyond the halo mass function and model the spatial distribution of galaxies and the topology of reionization within these alternative cosmologies. While full, high-resolution hydrodynamical simulations are an important long-term goal, their computational expense makes them impractical for exploring the vast and degenerate parameter space where both cosmological and astrophysical properties vary. A more immediate and powerful path forward lies in combining our analytical framework with efficient, large-volume semi-numerical codes.

To this end, we plan to integrate our model with `SCRIPT`, a semi-numerical model of galaxy formation and reionization developed by our group [135, 136]. This hybrid approach will enable us to self-consistently generate a rich set of mock observables, including galaxy luminosity functions, clustering statistics, the Lyman- $\alpha$  forest opacity, and the 21-cm signal, for a wide range of CPLn $\Lambda$ CDM and astrophysical scenarios. Confronting these detailed predictions with the wealth of data from JWST, and soon from the Roman Space Telescope and 21-cm experiments like the SKA, will be indispensable for decisively disentangling the signatures of new physics from the complexities of galaxy formation at cosmic dawn.

## Acknowledgments

AC and TRC acknowledge support from the Department of Atomic Energy, Government of India, under project no. 12-R&D-TFR-5.02-0700. AAS acknowledges funding from Anusandhan National Research Foundation (ANRF), Government of India, under the research grant no. CRG/2023/003984. PM acknowledges funding from the ANRF, Government of India, under the National Post-Doctoral Fellowship (File no. PDF/2023/001986).

## Data Availability

The data generated and presented in this paper will be made available upon reasonable request to the corresponding author (AC).



## A Constraints on the redshift evolution of galaxy properties from JWST UVLF observations in the $\Lambda$ CDM cosmological framework

In this appendix, we summarize the constraints (at 68% confidence level) obtained on the evolving astrophysical properties of high- $z$  galaxies from the available observational datasets discussed in Section 3. This model shall be referred to as the  **$\Lambda$ CDM+astro-evolution** model.

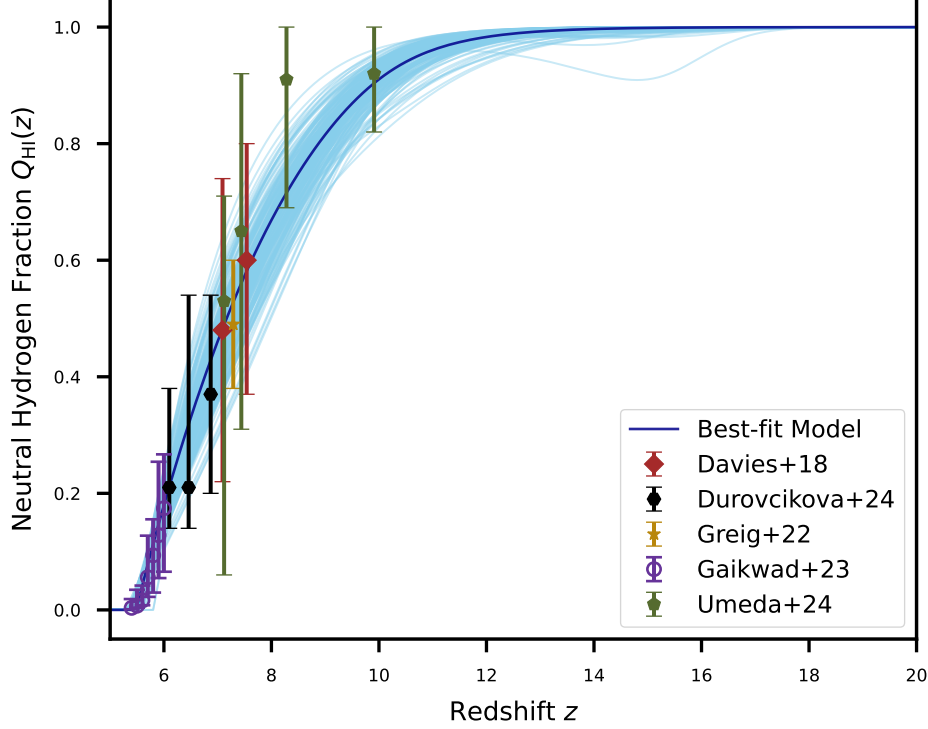


**Figure 10:** The evolution of the globally averaged intergalactic neutral hydrogen fraction as a function of redshift for 200 random samples drawn from the MCMC chains of the  **$\Lambda$ CDM+astro-evolution** model. The colored data points indicate the observational measurements of  $Q_{\text{HI}}(z)$  used in the analysis.

Here, we adopt the  $\Lambda$ CDM as background cosmological model, wherein the various cosmological parameters are assumed to have the values mentioned at the end of Section 1. The astrophysical parameters  $\log_{10}(\varepsilon_{*10,\text{UV}})$  and  $\alpha_*$  in this case are considered to evolve with redshift following a tanh parameterization, and can be expressed as

$$\log_{10} \varepsilon_{*10,\text{UV}}(z) = \frac{\ell_{\varepsilon,\text{hi}} + \ell_{\varepsilon,\text{lo}}}{2} + \frac{\ell_{\varepsilon,\text{hi}} - \ell_{\varepsilon,\text{lo}}}{2} \tanh\left(\frac{z - z_*}{\Delta z_*}\right), \quad (\text{A.1})$$

and

$$\alpha_*(z) = \frac{\alpha_{\text{hi}} + \alpha_{\text{lo}}}{2} + \frac{\alpha_{\text{hi}} - \alpha_{\text{lo}}}{2} \tanh\left(\frac{z - z_*}{\Delta z_*}\right). \quad (\text{A.2})$$

such that the parameter  $\log_{10} \varepsilon_{*10,\text{UV}}$  ( $\alpha_*$ ) asymptotes to  $\ell_{\varepsilon,\text{lo}}$  ( $\alpha_{\text{lo}}$ ) at low redshifts and to  $\ell_{\varepsilon,\text{hi}}$  ( $\alpha_{\text{hi}}$ ) at high redshifts, with the transition between these values occurring at a characteristic redshift  $z_*$  over a range  $\Delta z_*$ . The constraints on the nine free parameters

**Table 3:** Parameter constraints obtained from the MCMC-based analysis. The first nine rows correspond to the free parameters of the  $\Lambda$ CDM+**astro-evolution** model, while the remaining are the derived parameters. The free parameters are assumed to have uniform priors in the range mentioned in the second column. The numbers in the other columns show the mean value with  $1\sigma$  errors for different parameters of the model.

Parameters	Priors	68% limits
$\ell_{\varepsilon,\text{hi}}$	[-2.0, 2.0]	$-0.068_{-0.48}^{+0.044}$
$\ell_{\varepsilon,\text{lo}}$	[-2.0, 0.5]	$-0.889_{-0.045}^{+0.070}$
$z_*$	[8.0, 18.0]	$11.84_{-1.5}^{+0.38}$
$\Delta z_*$	[0.5, 6.0]	$1.89_{-0.94}^{+0.39}$
$\alpha_{\text{hi}}$	[0.0, 7.0]	$2.11_{-1.5}^{+0.15}$
$\alpha_{\text{lo}}$	[-1.0, 1.0]	$0.302_{-0.050}^{+0.036}$
$\log_{10}(\varepsilon_{\text{esc},10})$	[-3.0, 1.0]	$-0.810 \pm 0.043$
$\alpha_{\text{esc}}$	[-3.0, 1.0]	$-0.17_{-0.11}^{+0.14}$
$\log_{10}(M_{\text{crit}}/M_{\odot})$	[9.0, 11.0]	$10.11_{-0.11}^{+0.28}$
$\tau_{el}$	-	$0.0540_{-0.0023}^{+0.0020}$
$\ell_{\varepsilon,\text{hi}} - \ell_{\varepsilon,\text{lo}}$	-	$0.822_{-0.52}^{+0.014}$
$\alpha_{\text{hi}} - \alpha_{\text{lo}}$	-	$1.81_{-1.5}^{+0.15}$

characterizing the astrophysical properties of galaxies are mentioned in Table 3. The implications of these constraints have been discussed extensively in our earlier papers. We show the reionization history for 200 random samples drawn from the MCMC chains of  $\Lambda$ CDM+**astro-evolution** model in Figure 10 to serve as a benchmark for better understanding of the effect that changing the background cosmological model has on the process of reionization.

## B Constraints on the cosmological parameters in the $\text{CPL}n\Lambda\text{CDM}$ cosmology, as obtained by Mukherjee et al. (2025)

In this appendix, we list the constraints (at 68% confidence level) obtained by Mukherjee et al. (2025) [108] on the cosmological parameters of the  $\text{CPL}n\Lambda\text{CDM}$  model from a joint analysis of the full Planck-PR3 CMB TT, EE, TE and lensing data [6], DESI-BAO Data Release 1 measurements [133], and the Pantheon Plus compilation of SN-Ia light curves [134]. Here, we have removed the first 30% of the samples from their chains as burn-in and used the remaining samples to derive these constraints.

**Table 4:** Constraints on the cosmological model parameters obtained by jointly analyzing the full Planck-2018 CMB dataset (temperature, polarization, and lensing), the DESI BAO measurements, and the latest Pantheon-Plus compilation of light curves of spectroscopically confirmed Type Ia supernovae.

P18 + DESI-DR1 + PP (68% limits)			
Sampled Parameters		Derived Parameters	
$\log(10^{10} A_s)$	$3.041 \pm 0.014$	$A_s$	$(2.093 \pm 0.030) \times 10^{-9}$
$n_s$	$0.9657 \pm 0.0038$	$H_0$	$68.03 \pm 0.73$
$100\theta_s$	$1.04190 \pm 0.00029$	$\Omega_m$	$0.3081 \pm 0.0068$
$\Omega_b h^2$	$0.02240 \pm 0.00014$	$\Omega_\Lambda$	$-0.680^{+0.78}_{-0.058}$
$\Omega_c h^2$	$0.11948 \pm 0.00099$	$\sigma_8$	$0.816 \pm 0.010$
$\tau_{\text{reion}}$	$0.0536 \pm 0.0073$	$S_8$	$0.827 \pm 0.010$
$w_0$	$-0.887^{+0.039}_{-0.087}$	$r_{\text{drag}}$	$147.21 \pm 0.24$
$w_a$	$-0.47^{+0.37}_{-0.15}$	$\Omega_b$	$0.0484 \pm 0.0011$
$\Omega_\phi$	$< 1.41$		

## C A $\text{CPL}n\Lambda\text{CDM}$ model that maximizes the boost in halo abundance (relative to $\Lambda\text{CDM}$ ) at $z \approx 13.2$ compared to $z \approx 5$

In this appendix, we carry out an MCMC analysis similar to that done in Section 4.2, except that we now select the  $\text{CPL}n\Lambda\text{CDM}$  cosmological model that maximizes the ratio of the enhancement in the abundance of dark matter halos of fixed mass (relative to the baseline  $\Lambda\text{CDM}$  (Planck 2018) model) at  $z \approx 13.2$  to that at  $z = 5$ . We shall refer to this as the “**relative-zboost  $\text{CPL}n\Lambda\text{CDM}$** ” model, whose corresponding cosmological parameters are listed in Table 5. The enhancement in halo number densities relative to the  $\Lambda\text{CDM}$  model for this scenario is presented in Figure 11. The corresponding UV luminosity functions, derived for 200 random samples from the MCMC analysis, are shown in Figure 12. As evident from these figures, we find the results for this analysis to be qualitatively similar to those obtained in Section 4.2, thereby raising considerable apprehension on the viability of  $\text{CPL}n\Lambda\text{CDM}$  models as an explanation for the excess galaxies detected by JWST at  $z > 10$ .

**Table 5:** Cosmological parameters for the  $\text{CPL}n\Lambda\text{CDM}$  model that remains consistent with other cosmological observations and yields the largest enhancement in the abundance of dark matter halos w.r.t. the baseline  $\Lambda\text{CDM}$  (Planck 2018) model, at  $z = 13.2$  compared to that at  $z = 5$

$\Omega_m$	$\Omega_b h^2$	$\Omega_\Lambda$	$h$	$\Omega_\phi$
0.320444	0.0220481	-1.38512	0.66883	2.06459
$w_0$	$w_a$	$n_s$	$\sigma_8$	$\tau_{\text{el}}$
-0.956524	-0.165338	0.970466	0.834091	0.0750381

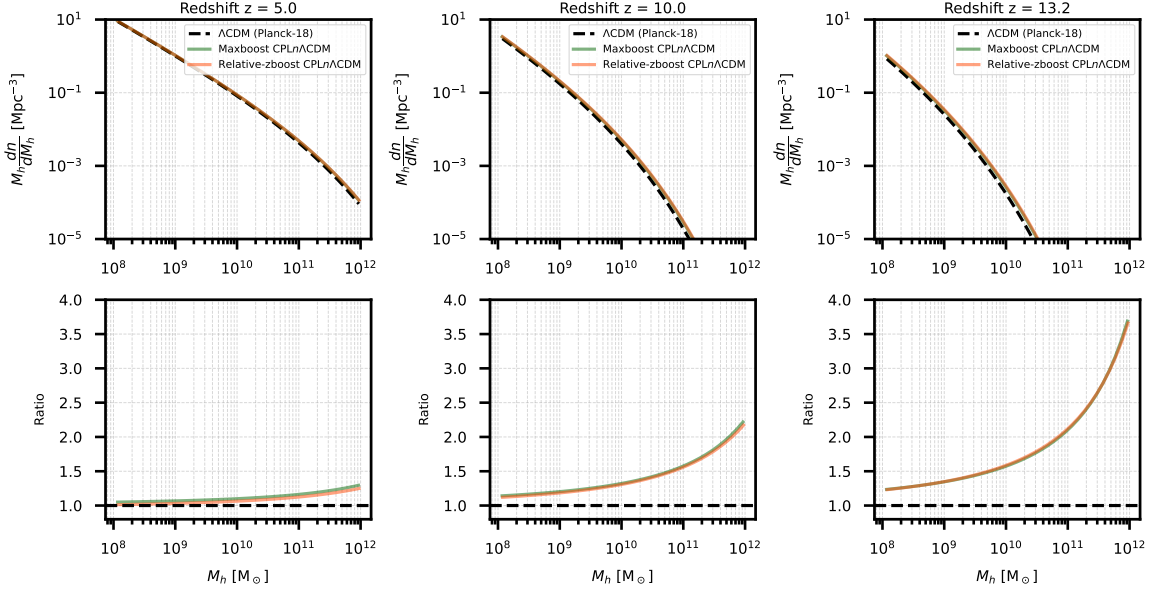


**Figure 11:** Comparison of the dark matter halo mass functions at high redshifts ( $z = 5, 10$ , and  $13.2$ ) within the **maxboost  $\text{CPL}n\Lambda\text{CDM}$**  and **relative-zboost  $\text{CPL}n\Lambda\text{CDM}$**  models with that obtained for the baseline  $\Lambda\text{CDM}$  (Planck 2018) cosmological model.

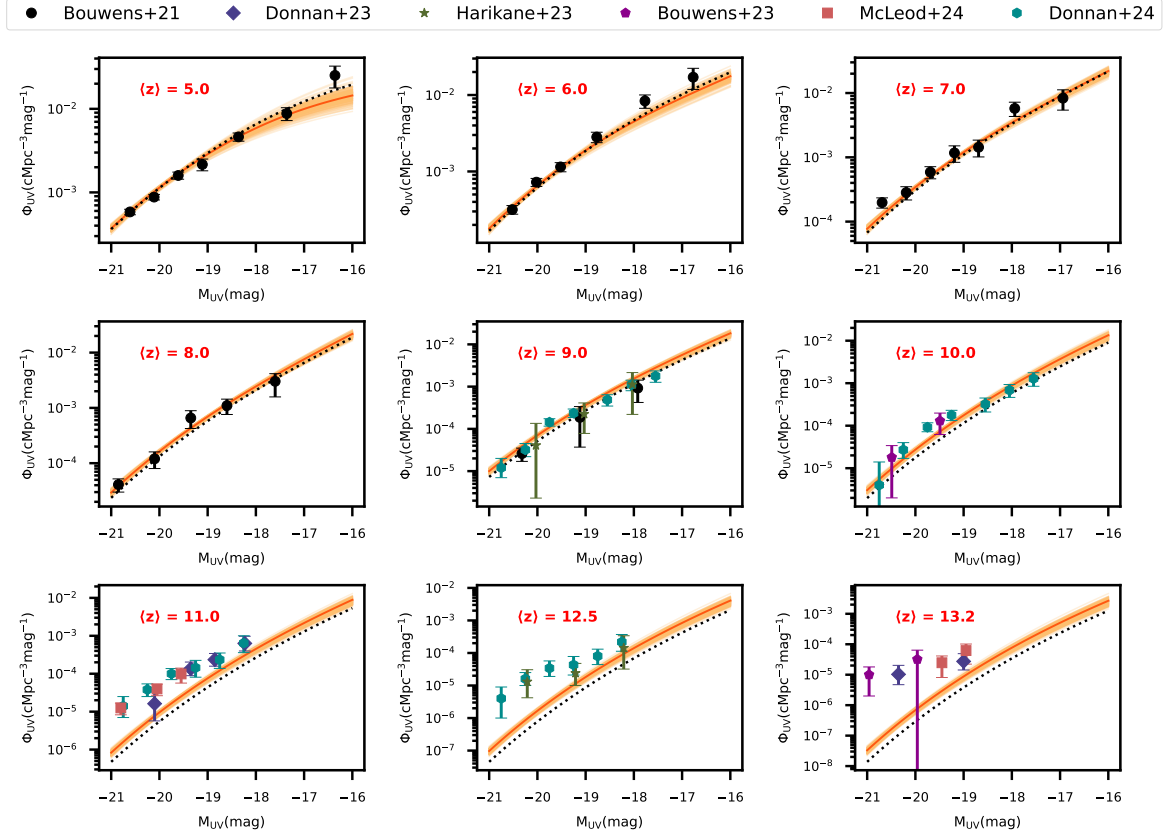


**Figure 12:** The galaxy UV luminosity functions at nine different redshifts (with their respective mean values  $\langle z \rangle$  mentioned in the upper left corner) for 200 random samples drawn from the MCMC chains of the **relative-zboost CPL $n$  $\Lambda$ CDM** model. In each panel, the solid dark-orange line corresponds to the best-fit model, while the colored data points show the different observational constraints [33–36, 128, 129] used in the likelihood analysis. The prediction from a model within the  $\Lambda$ CDM (Planck-2018) cosmology that best matches the observational measurements at  $z < 10$  and does not assume any evolution in the UV efficiency parameters above  $z \sim 10$  is also shown using black dotted lines.

## References

- [1] G.F. Smoot, C.L. Bennett, A. Kogut, E.L. Wright, J. Aymon, N.W. Boggess et al., *Structure in the COBE Differential Microwave Radiometer First-Year Maps*, [ApJ \*\*396\*\* \(1992\) L1](#).
- [2] D.N. Spergel, R. Bean, O. Doré, M.R. Nolta, C.L. Bennett, J. Dunkley et al., *Three-Year Wilkinson Microwave Anisotropy Probe (WMAP) Observations: Implications for Cosmology*, [ApJS \*\*170\*\* \(2007\) 377](#) [[astro-ph/0603449](#)].
- [3] C.L. Bennett, D. Larson, J.L. Weiland, N. Jarosik, G. Hinshaw, N. Odegard et al., *Nine-year Wilkinson Microwave Anisotropy Probe (WMAP) Observations: Final Maps and Results*, [ApJS \*\*208\*\* \(2013\) 20](#) [[1212.5225](#)].
- [4] Planck Collaboration, P.A.R. Ade, N. Aghanim, C. Armitage-Caplan, M. Arnaud, M. Ashdown et al., *Planck 2013 results. XVI. Cosmological parameters*, [A&A \*\*571\*\* \(2014\) A16](#) [[1303.5076](#)].

- [5] Planck Collaboration, P.A.R. Ade, N. Aghanim, M. Arnaud, M. Ashdown, J. Aumont et al., *Planck 2015 results. XIII. Cosmological parameters*, [A&A \*\*594\*\* \(2016\) A13 \[1502.01589\]](#).
- [6] Planck Collaboration, N. Aghanim, Y. Akrami, M. Ashdown, J. Aumont, C. Baccigalupi et al., *Planck 2018 results. VI. Cosmological parameters*, [A&A \*\*641\*\* \(2020\) A6 \[1807.06209\]](#).
- [7] G. Steigman, *Primordial Nucleosynthesis in the Precision Cosmology Era*, [Annual Review of Nuclear and Particle Science \*\*57\*\* \(2007\) 463 \[0712.1100\]](#).
- [8] R.H. Cyburt, B.D. Fields, K.A. Olive and T.-H. Yeh, *Big bang nucleosynthesis: Present status*, [Reviews of Modern Physics \*\*88\*\* \(2016\) 015004 \[1505.01076\]](#).
- [9] R.J. Cooke, M. Pettini and C.C. Steidel, *One Percent Determination of the Primordial Deuterium Abundance*, [ApJ \*\*855\*\* \(2018\) 102 \[1710.11129\]](#).
- [10] S. Cole, W.J. Percival, J.A. Peacock, P. Norberg, C.M. Baugh, C.S. Frenk et al., *The 2dF Galaxy Redshift Survey: power-spectrum analysis of the final data set and cosmological implications*, [MNRAS \*\*362\*\* \(2005\) 505 \[astro-ph/0501174\]](#).
- [11] D.J. Eisenstein, I. Zehavi, D.W. Hogg, R. Scoccimarro, M.R. Blanton, R.C. Nichol et al., *Detection of the Baryon Acoustic Peak in the Large-Scale Correlation Function of SDSS Luminous Red Galaxies*, [ApJ \*\*633\*\* \(2005\) 560 \[astro-ph/0501171\]](#).
- [12] É. Aubourg, S. Bailey, J.E. Bautista, F. Beutler, V. Bhardwaj, D. Bizyaev et al., *Cosmological implications of baryon acoustic oscillation measurements*, [Phys. Rev. D \*\*92\*\* \(2015\) 123516 \[1411.1074\]](#).
- [13] S. Alam, M. Ata, S. Bailey, F. Beutler, D. Bizyaev, J.A. Blazek et al., *The clustering of galaxies in the completed SDSS-III Baryon Oscillation Spectroscopic Survey: cosmological analysis of the DR12 galaxy sample*, [MNRAS \*\*470\*\* \(2017\) 2617 \[1607.03155\]](#).
- [14] G. Efstathiou, W.J. Sutherland and S.J. Maddox, *The cosmological constant and cold dark matter*, [Nature \*\*348\*\* \(1990\) 705](#).
- [15] A.G. Riess, A.V. Filippenko, P. Challis, A. Clocchiatti, A. Diercks, P.M. Garnavich et al., *Observational Evidence from Supernovae for an Accelerating Universe and a Cosmological Constant*, [AJ \*\*116\*\* \(1998\) 1009 \[astro-ph/9805201\]](#).
- [16] S. Perlmutter, G. Aldering, G. Goldhaber, R.A. Knop, P. Nugent, P.G. Castro et al., *Measurements of  $\Omega$  and  $\Lambda$  from 42 High-Redshift Supernovae*, [ApJ \*\*517\*\* \(1999\) 565 \[astro-ph/9812133\]](#).
- [17] D.H. Weinberg, M.J. Mortonson, D.J. Eisenstein, C. Hirata, A.G. Riess and E. Rozo, *Observational probes of cosmic acceleration*, [Phys. Rep. \*\*530\*\* \(2013\) 87 \[1201.2434\]](#).
- [18] M. Betoule, R. Kessler, J. Guy, J. Mosher, D. Hardin, R. Biswas et al., *Improved cosmological constraints from a joint analysis of the SDSS-II and SNLS supernova samples*, [A&A \*\*568\*\* \(2014\) A22 \[1401.4064\]](#).
- [19] D.M. Scolnic, D.O. Jones, A. Rest, Y.C. Pan, R. Chornock, R.J. Foley et al., *The Complete Light-curve Sample of Spectroscopically Confirmed SNe Ia from Pan-STARRS1 and Cosmological Constraints from the Combined Pantheon Sample*, [ApJ \*\*859\*\* \(2018\) 101 \[1710.00845\]](#).
- [20] T.M.C. Abbott, S. Allam, P. Andersen, C. Angus, J. Asorey, A. Avelino et al., *First Cosmology Results using Type Ia Supernovae from the Dark Energy Survey: Constraints on Cosmological Parameters*, [ApJ \*\*872\*\* \(2019\) L30 \[1811.02374\]](#).
- [21] R.P. Naidu, P.A. Oesch, P. van Dokkum, E.J. Nelson, K.A. Suess, G. Brammer et al., *Two Remarkably Luminous Galaxy Candidates at  $z \approx 10$ -12 Revealed by JWST*, [ApJ \*\*940\*\* \(2022\) L14 \[2207.09434\]](#).

- [22] M. Castellano, A. Fontana, T. Treu, P. Santini, E. Merlin, N. Leethochawalit et al., *Early Results from GLASS-JWST. III. Galaxy Candidates at  $z$  9-15*, [\*ApJ\* \*\*938\*\* \(2022\) L15](#) [[2207.09436](#)].
- [23] S.L. Finkelstein, M.B. Bagley, P. Arrabal Haro, M. Dickinson, H.C. Ferguson, J.S. Kartaltepe et al., *A Long Time Ago in a Galaxy Far, Far Away: A Candidate  $z \sim 12$  Galaxy in Early JWST CEERS Imaging*, [\*ApJ\* \*\*940\*\* \(2022\) L55](#) [[2207.12474](#)].
- [24] I. Labbé, P. van Dokkum, E. Nelson, R. Bezanson, K.A. Suess, J. Leja et al., *A population of red candidate massive galaxies 600 Myr after the Big Bang*, [\*Nature\* \*\*616\*\* \(2023\) 266](#) [[2207.12446](#)].
- [25] H. Atek, M. Shuntov, L.J. Furtak, J. Richard, J.-P. Kneib, G. Mahler et al., *Revealing galaxy candidates out to  $z$  16 with JWST observations of the lensing cluster SMACS0723*, [\*MNRAS\* \*\*519\*\* \(2023\) 1201](#) [[2207.12338](#)].
- [26] N.J. Adams, C.J. Conselice, L. Ferreira, D. Austin, J.A.A. Trussler, I. Juodžbalis et al., *Discovery and properties of ultra-high redshift galaxies ( $9 < z < 12$ ) in the JWST ERO SMACS 0723 Field*, [\*MNRAS\* \*\*518\*\* \(2023\) 4755](#) [[2207.11217](#)].
- [27] L.D. Bradley, D. Coe, G. Brammer, L.J. Furtak, R.L. Larson, V. Kokorev et al., *High-redshift Galaxy Candidates at  $z = 9$ -10 as Revealed by JWST Observations of WHL0137-08*, [\*ApJ\* \*\*955\*\* \(2023\) 13](#) [[2210.01777](#)].
- [28] L. Whitler, R. Endsley, D.P. Stark, M. Topping, Z. Chen and S. Charlot, *On the ages of bright galaxies 500 Myr after the big bang: insights into star formation activity at  $z \gtrsim 15$  with JWST*, [\*MNRAS\* \*\*519\*\* \(2023\) 157](#) [[2208.01599](#)].
- [29] B. Robertson, B.D. Johnson, S. Tacchella, D.J. Eisenstein, K. Hainline, S. Arribas et al., *Earliest Galaxies in the JADES Origins Field: Luminosity Function and Cosmic Star Formation Rate Density 300 Myr after the Big Bang*, [\*ApJ\* \*\*970\*\* \(2024\) 31](#) [[2312.10033](#)].
- [30] M. Castellano, A. Fontana, T. Treu, E. Merlin, P. Santini, P. Bergamini et al., *Early Results from GLASS-JWST. XIX. A High Density of Bright Galaxies at  $z \approx 10$  in the A2744 Region*, [\*ApJ\* \*\*948\*\* \(2023\) L14](#) [[2212.06666](#)].
- [31] S.L. Finkelstein, M.B. Bagley, H.C. Ferguson, S.M. Wilkins, J.S. Kartaltepe, C. Papovich et al., *CEERS Key Paper. I. An Early Look into the First 500 Myr of Galaxy Formation with JWST*, [\*ApJ\* \*\*946\*\* \(2023\) L13](#) [[2211.05792](#)].
- [32] P.G. Pérez-González, L. Costantin, D. Langeroodi, P. Rinaldi, M. Annunziatella, O. Ilbert et al., *Life beyond 30: Probing the  $-20 < M_{UV} < -17$  Luminosity Function at  $8 < z < 13$  with the NIRCam Parallel Field of the MIRI Deep Survey*, [\*ApJ\* \*\*951\*\* \(2023\) L1](#) [[2302.02429](#)].
- [33] C.T. Donnan, D.J. McLeod, J.S. Dunlop, R.J. McLure, A.C. Carnall, R. Begley et al., *The evolution of the galaxy UV luminosity function at redshifts  $z = 8 - 15$  from deep JWST and ground-based near-infrared imaging*, [\*MNRAS\* \*\*518\*\* \(2023\) 6011](#) [[2207.12356](#)].
- [34] Y. Harikane, M. Ouchi, M. Oguri, Y. Ono, K. Nakajima, Y. Isobe et al., *A Comprehensive Study of Galaxies at  $z$  9-16 Found in the Early JWST Data: Ultraviolet Luminosity Functions and Cosmic Star Formation History at the Pre-reionization Epoch*, [\*ApJS\* \*\*265\*\* \(2023\) 5](#) [[2208.01612](#)].
- [35] R. Bouwens, G. Illingworth, P. Oesch, M. Stefanon, R. Naidu, I. van Leeuwen et al., *UV luminosity density results at  $z < 8$  from the first JWST/NIRCam fields: limitations of early data sets and the need for spectroscopy*, [\*MNRAS\* \*\*523\*\* \(2023\) 1009](#) [[2212.06683](#)].
- [36] D.J. McLeod, C.T. Donnan, R.J. McLure, J.S. Dunlop, D. Magee, R. Begley et al., *The galaxy UV luminosity function at  $z \simeq 11$  from a suite of public JWST ERS, ERO, and Cycle-1 programs*, [\*MNRAS\* \*\*527\*\* \(2024\) 5004](#) [[2304.14469](#)].



- [37] N.J. Adams, C.J. Conselice, D. Austin, T. Harvey, L. Ferreira, J. Trussler et al., *EPOCHS. II. The Ultraviolet Luminosity Function from  $7.5 < z < 13.5$  Using  $180 \text{ arcmin}^2$  of Deep, Blank Fields from the PEARLS Survey and Public JWST Data*, *ApJ* **965** (2024) 169 [2304.13721].
- [38] S.L. Finkelstein, G.C.K. Leung, M.B. Bagley, M. Dickinson, H.C. Ferguson, C. Papovich et al., *The Complete CEERS Early Universe Galaxy Sample: A Surprisingly Slow Evolution of the Space Density of Bright Galaxies at  $z \sim 8.5\text{--}14.5$* , *ApJ* **969** (2024) L2 [2311.04279].
- [39] L. Whitler, D.P. Stark, M.W. Topping, B. Robertson, M. Rieke, K.N. Hainline et al., *The zrsim9 galaxy UV luminosity function from the JWST Advanced Deep Extragalactic Survey: insights into early galaxy evolution and reionization*, *arXiv e-prints* (2025) arXiv:2501.00984 [2501.00984].
- [40] P.G. Pérez-González, G. Östlin, L. Costantin, J. Melinder, S.L. Finkelstein, R.S. Somerville et al., *The rise of the galactic empire: luminosity functions at  $z \sim 17$  and  $z \sim 25$  estimated with the MIDIS+NGDEEP ultra-deep JWST/NIRCam dataset*, *arXiv e-prints* (2025) arXiv:2503.15594 [2503.15594].
- [41] A. Weibel, P.A. Oesch, C.C. Williams, C.K. Jespersen, M. Shuntov, K.E. Whitaker et al., *Exploring Cosmic Dawn with PANORAMIC I: The Bright End of the UVLF at  $z \sim 9\text{--}17$* , *arXiv e-prints* (2025) arXiv:2507.06292 [2507.06292].
- [42] M. Haslbauer, P. Kroupa, A.H. Zonoozi and H. Haghi, *Has JWST Already Falsified Dark-matter-driven Galaxy Formation?*, *ApJ* **939** (2022) L31 [2210.14915].
- [43] C.C. Lovell, I. Harrison, Y. Harikane, S. Tacchella and S.M. Wilkins, *Extreme value statistics of the halo and stellar mass distributions at high redshift: are JWST results in tension with  $\Lambda$ CDM?*, *MNRAS* **518** (2023) 2511 [2208.10479].
- [44] M. Boylan-Kolchin, *Stress testing  $\Lambda$ CDM with high-redshift galaxy candidates*, *Nature Astronomy* **7** (2023) 731 [2208.01611].
- [45] A. Dekel, K.S. Sarkar, Y. Birnboim, N. Mandelker and Z. Li, *Efficient Formation of Massive Galaxies at Cosmic Dawn by Feedback-Free Starbursts*, *arXiv e-prints* (2023) arXiv:2303.04827 [2303.04827].
- [46] Z. Li, A. Dekel, K.C. Sarkar, H. Aung, M. Giavalisco, N. Mandelker et al., *Feedback-free starbursts at cosmic dawn: Observable predictions for JWST*, *A&A* **690** (2024) A108 [2311.14662].
- [47] Y. Qin, S. Balu and J.S.B. Wyithe, *Implications of  $z \gtrsim 12$  JWST galaxies for galaxy formation at high redshift*, *MNRAS* **526** (2023) 1324 [2305.17959].
- [48] A. Chakraborty and T.R. Choudhury, *Modelling the star-formation activity and ionizing properties of high-redshift galaxies*, *J. Cosmology Astropart. Phys.* **2024** (2024) 078 [2404.02879].
- [49] A. Chakraborty and T.R. Choudhury, *Probing Reionization-Era Galaxies with JWST UV Luminosity Functions and Large-Scale Clustering*, *arXiv e-prints* (2025) arXiv:2503.07590 [2503.07590].
- [50] J. Mirocha and S.R. Furlanetto, *Balancing the efficiency and stochasticity of star formation with dust extinction in  $z > 10$  galaxies observed by JWST*, *MNRAS* **519** (2023) 843 [2208.12826].
- [51] C.A. Mason, M. Trenti and T. Treu, *The brightest galaxies at cosmic dawn*, *MNRAS* **521** (2023) 497 [2207.14808].
- [52] X. Shen, M. Vogelsberger, M. Boylan-Kolchin, S. Tacchella and R. Kannan, *The impact of UV variability on the abundance of bright galaxies at  $z \geq 9$* , *MNRAS* **525** (2023) 3254 [2305.05679].

- [53] G. Sun, C.-A. Faucher-Giguère, C.C. Hayward, X. Shen, A. Wetzel and R.K. Cochrane, *Bursty Star Formation Naturally Explains the Abundance of Bright Galaxies at Cosmic Dawn*, [\*ApJ\* \*\*955\*\* \(2023\) L35](#) [[2307.15305](#)].
- [54] A. Pallottini and A. Ferrara, *Stochastic star formation in early galaxies: JWST implications*, [\*arXiv e-prints\* \(2023\) arXiv:2307.03219](#) [[2307.03219](#)].
- [55] V. Gelli, C. Mason and C.C. Hayward, *The Impact of Mass-dependent Stochasticity at Cosmic Dawn*, [\*ApJ\* \*\*975\*\* \(2024\) 192](#) [[2405.13108](#)].
- [56] A. Kravtsov and V. Belokurov, *Stochastic star formation and the abundance of  $z > 10$  UV-bright galaxies*, [\*arXiv e-prints\* \(2024\) arXiv:2405.04578](#) [[2405.04578](#)].
- [57] K. Inayoshi, Y. Harikane, A.K. Inoue, W. Li and L.C. Ho, *A Lower Bound of Star Formation Activity in Ultra-high-redshift Galaxies Detected with JWST: Implications for Stellar Populations and Radiation Sources*, [\*ApJ\* \*\*938\*\* \(2022\) L10](#) [[2208.06872](#)].
- [58] A. Trinca, R. Schneider, R. Valiante, L. Graziani, A. Ferrotti, K. Omukai et al., *Exploring the nature of UV-bright *zrsim10* galaxies detected by JWST: star formation, black hole accretion, or a non-universal IMF?*, [\*arXiv e-prints\* \(2023\) arXiv:2305.04944](#) [[2305.04944](#)].
- [59] E.M. Ventura, Y. Qin, S. Balu and J.S.B. Wyithe, *Semi-analytic modelling of Pop. III star formation and metallicity evolution - I. Impact on the UV luminosity functions at  $z = 9-16$* , [\*MNRAS\* \*\*529\*\* \(2024\) 628](#) [[2401.07396](#)].
- [60] L.Y.A. Yung, R.S. Somerville, S.L. Finkelstein, S.M. Wilkins and J.P. Gardner, *Are the ultra-high-redshift galaxies at  $z \gtrsim 10$  surprising in the context of standard galaxy formation models?*, [\*MNRAS\* \*\*527\*\* \(2024\) 5929](#) [[2304.04348](#)].
- [61] A. Hutter, E.R. Cueto, P. Dayal, S. Gottlöber, M. Trebitsch and G. Yepes, *ASTRAEUS: X. Indications of a top-heavy initial mass function in highly star-forming galaxies from JWST observations at  $z \gtrsim 10$* , [\*A&A\* \*\*694\*\* \(2025\) A254](#) [[2410.00730](#)].
- [62] S. Lu, C.S. Frenk, S. Bose, C.G. Lacey, S. Cole, C.M. Baugh et al., *A comparison of pre-existing  $\Lambda$ CDM predictions with the abundance of JWST galaxies at high redshift*, [\*MNRAS\* \*\*536\*\* \(2025\) 1018](#) [[2406.02672](#)].
- [63] A. Ferrara, A. Pallottini and P. Dayal, *On the stunning abundance of super-early, luminous galaxies revealed by JWST*, [\*MNRAS\* \*\*522\*\* \(2023\) 3986](#) [[2208.00720](#)].
- [64] F. Ziparo, A. Ferrara, L. Sommovigo and M. Kohandel, *Blue monsters. Why are JWST super-early, massive galaxies so blue?*, [\*MNRAS\* \*\*520\*\* \(2023\) 2445](#) [[2209.06840](#)].
- [65] A. Ferrara, *Super-early JWST galaxies, outflows, and Ly $\alpha$  visibility in the Epoch of Reionization*, [\*A&A\* \*\*684\*\* \(2024\) A207](#) [[2310.12197](#)].
- [66] A. Ferrara, A. Pallottini and L. Sommovigo, *Blue monsters at  $z \gtrsim 10$ : Where all their dust has gone*, [\*A&A\* \*\*694\*\* \(2025\) A286](#) [[2410.19042](#)].
- [67] F. Pacucci, P. Dayal, Y. Harikane, A.K. Inoue and A. Loeb, *Are the newly-discovered  $z \gtrsim 13$  drop-out sources starburst galaxies or quasars?*, [\*MNRAS\* \*\*514\*\* \(2022\) L6](#) [[2201.00823](#)].
- [68] S. Hegde, M.M. Wyatt and S.R. Furlanetto, *A hidden population of active galactic nuclei can explain the overabundance of luminous  $z \gtrsim 10$  objects observed by JWST*, [\*J. Cosmology Astropart. Phys.\* \*\*2024\*\* \(2024\) 025](#) [[2405.01629](#)].
- [69] S. Fujimoto, B. Wang, J.R. Weaver, V. Kokorev, H. Atek, R. Bezanson et al., *UNCOVER: A NIRSpect Census of Lensed Galaxies at  $z = 8.50-13.08$  Probing a High-AGN Fraction and Ionized Bubbles in the Shadow*, [\*ApJ\* \*\*977\*\* \(2024\) 250](#) [[2308.11609](#)].
- [70] X. Shen, M. Vogelsberger, M. Boylan-Kolchin, S. Tacchella and R.P. Naidu, *Early galaxies and early dark energy: a unified solution to the hubble tension and puzzles of massive bright galaxies revealed by JWST*, [\*MNRAS\* \*\*533\*\* \(2024\) 3923](#) [[2406.15548](#)].

- [71] W. Liu, H. Zhan, Y. Gong and X. Wang, *Can early dark energy be probed by the high-redshift galaxy abundance?*, *MNRAS* **533** (2024) 860 [[2402.14339](#)].
- [72] Y. Gong, B. Yue, Y. Cao and X. Chen, *Fuzzy Dark Matter as a Solution to Reconcile the Stellar Mass Density of High- $z$  Massive Galaxies and Reionization History*, *ApJ* **947** (2023) 28 [[2209.13757](#)].
- [73] S. Bird, C.-F. Chang, Y. Cui and D. Yang, *Enhanced early galaxy formation in JWST from axion dark matter?*, *Physics Letters B* **858** (2024) 139062 [[2307.10302](#)].
- [74] B. Liu and V. Bromm, *Accelerating Early Massive Galaxy Formation with Primordial Black Holes*, *ApJ* **937** (2022) L30 [[2208.13178](#)].
- [75] G. Hütsi, M. Raidal, J. Urrutia, V. Vaskonen and H. Veermäe, *Did JWST observe imprints of axion miniclusters or primordial black holes?*, *Phys. Rev. D* **107** (2023) 043502 [[2211.02651](#)].
- [76] G.-W. Yuan, L. Lei, Y.-Z. Wang, B. Wang, Y.-Y. Wang, C. Chen et al., *Rapidly growing primordial black holes as seeds of the massive high-redshift JWST Galaxies*, *Science China Physics, Mechanics, and Astronomy* **67** (2024) 109512 [[2303.09391](#)].
- [77] A. Matteri, A. Pallottini and A. Ferrara, *Can primordial black holes explain the overabundance of bright super-early galaxies?*, *A&A* **697** (2025) A65 [[2503.01968](#)].
- [78] M. Biagetti, G. Franciolini and A. Riotto, *High-redshift JWST Observations and Primordial Non-Gaussianity*, *ApJ* **944** (2023) 113 [[2210.04812](#)].
- [79] P. Parashari and R. Laha, *Primordial power spectrum in light of JWST observations of high redshift galaxies*, *MNRAS* **526** (2023) L63 [[2305.00999](#)].
- [80] S. Hirano and N. Yoshida, *Early Structure Formation from Primordial Density Fluctuations with a Blue, Tilted Power Spectrum: High-redshift Galaxies*, *ApJ* **963** (2024) 2 [[2306.11993](#)].
- [81] H. Padmanabhan and A. Loeb, *Alleviating the Need for Exponential Evolution of JWST Galaxies in  $10^{10} M_{\odot}$  Haloes at  $z \gtrsim 10$  by a Modified  $\Lambda$ CDM Power Spectrum*, *ApJ* **953** (2023) L4 [[2306.04684](#)].
- [82] N. Sabti, J.B. Muñoz and M. Kamionkowski, *Insights from HST into Ultramassive Galaxies and Early-Universe Cosmology*, *Phys. Rev. Lett.* **132** (2024) 061002 [[2305.07049](#)].
- [83] Y. Gouttenoire, S. Trifinopoulos, G. Valogiannis and M. Vanvlasselaer, *Scrutinizing the primordial black hole interpretation of PTA gravitational waves and JWST early galaxies*, *Phys. Rev. D* **109** (2024) 123002 [[2307.01457](#)].
- [84] P.J.E. Peebles, *The large-scale structure of the universe* (1980).
- [85] J.A. Peacock, *Cosmological Physics* (1999).
- [86] S. Dodelson and F. Schmidt, *Modern Cosmology* (2020), [10.1016/C2017-0-01943-2](#).
- [87] T. Padmanabhan, *Theoretical Astrophysics - Volume 3, Galaxies and Cosmology*, vol. 3 (2002), [10.2277/0521562422](#).
- [88] S. Weinberg, *The cosmological constant problem*, *Reviews of Modern Physics* **61** (1989) 1.
- [89] T. Padmanabhan, *Cosmological constant-the weight of the vacuum*, *Phys. Rep.* **380** (2003) 235 [[hep-th/0212290](#)].
- [90] U.H. Danielsson and T.V. Riet, *What if string theory has no de Sitter vacua?*, *International Journal of Modern Physics D* **27** (2018) 1830007 [[1804.01120](#)].
- [91] C. Vafa, *The String Landscape and the Swampland*, *arXiv e-prints* (2005) [hep-th/0509212](#).
- [92] E. Palti, *The Swampland: Introduction and Review*, *Fortschritte der Physik* **67** (2019) 1900037 [[1903.06239](#)].

- [93] P. Agrawal, G. Obied, P.J. Steinhardt and C. Vafa, *On the cosmological implications of the string Swampland*, *Physics Letters B* **784** (2018) 271 [[1806.09718](#)].
- [94] G. Obied, H. Ooguri, L. Spodyneiko and C. Vafa, *De Sitter Space and the Swampland*, *arXiv e-prints* (2018) [arXiv:1806.08362](#) [[1806.08362](#)].
- [95] M. Cicoli, S. de Alwis, A. Maharana, F. Muia and F. Quevedo, *De Sitter vs Quintessence in String Theory*, *Fortschritte der Physik* **67** (2019) 1800079 [[1808.08967](#)].
- [96] M. Cicoli, F. Cunillera, A. Padilla and F.G. Pedro, *Quintessence and the Swampland: The Numerically Controlled Regime of Moduli Space*, *Fortschritte der Physik* **70** (2022) 2200008 [[2112.10783](#)].
- [97] J. Maldacena, *The Large- $N$  Limit of Superconformal Field Theories and Supergravity*, *International Journal of Theoretical Physics* **38** (1999) 1113 [[hep-th/9711200](#)].
- [98] R. Cardenas, T. Gonzalez, Y. Leiva, O. Martin and I. Quiros, *Model of the universe including dark energy accounted for by both a quintessence field and a (negative) cosmological constant*, *Phys. Rev. D* **67** (2003) 083501 [[astro-ph/0206315](#)].
- [99] K. Dutta, Ruchika, A. Roy, A.A. Sen and M.M. Sheikh-Jabbari, *Beyond  $\Lambda$ CDM with Low and High Redshift Data: Implications for Dark Energy*, *arXiv e-prints* (2018) [arXiv:1808.06623](#) [[1808.06623](#)].
- [100] L. Visinelli, S. Vagnozzi and U. Danielsson, *Revisiting a Negative Cosmological Constant from Low-Redshift Data*, *Symmetry* **11** (2019) 1035 [[1907.07953](#)].
- [101] E. Di Valentino, A. Mukherjee and A.A. Sen, *Dark Energy with Phantom Crossing and the  $H_0$  Tension*, *Entropy* **23** (2021) 404 [[2005.12587](#)].
- [102] Ö. Akarsu, J.D. Barrow, L.A. Escamilla and J.A. Vazquez, *Graduated dark energy: Observational hints of a spontaneous sign switch in the cosmological constant*, *Phys. Rev. D* **101** (2020) 063528 [[1912.08751](#)].
- [103] R. Calderón, R. Gannouji, B. L’Huillier and D. Polarski, *Negative cosmological constant in the dark sector?*, *Phys. Rev. D* **103** (2021) 023526 [[2008.10237](#)].
- [104] A.A. Sen, S.A. Adil and S. Sen, *Do cosmological observations allow a negative  $\Lambda$ ?*, *MNRAS* **518** (2023) 1098 [[2112.10641](#)].
- [105] S.A. Adil, U. Mukhopadhyay, A.A. Sen and S. Vagnozzi, *Dark energy in light of the early JWST observations: case for a negative cosmological constant?*, *J. Cosmology Astropart. Phys.* **2023** (2023) 072 [[2307.12763](#)].
- [106] S.A. Adil, Ö. Akarsu, E. Di Valentino, R.C. Nunes, E. Özülker, A.A. Sen et al., *Omnipotent dark energy: A phenomenological answer to the Hubble tension*, *Phys. Rev. D* **109** (2024) 023527 [[2306.08046](#)].
- [107] H. Wang, Z.-Y. Peng and Y.-S. Piao, *Can recent DESI BAO measurements accommodate a negative cosmological constant?*, *Phys. Rev. D* **111** (2025) L061306 [[2406.03395](#)].
- [108] P. Mukherjee, D. Kumar and A.A. Sen, *Quintessential Implications of the presence of AdS in the Dark Energy sector*, *arXiv e-prints* (2025) [arXiv:2501.18335](#) [[2501.18335](#)].
- [109] N. Menci, S.A. Adil, U. Mukhopadhyay, A.A. Sen and S. Vagnozzi, *Negative cosmological constant in the dark energy sector: tests from JWST photometric and spectroscopic observations of high-redshift galaxies*, *J. Cosmology Astropart. Phys.* **2024** (2024) 072 [[2401.12659](#)].
- [110] N. Menci, A.A. Sen and M. Castellano, *The Excess of JWST Bright Galaxies: A Possible Origin in the Ground State of Dynamical Dark Energy in the Light of DESI 2024 Data*, *ApJ* **976** (2024) 227 [[2410.22940](#)].

- [111] J.H. Wise, V.G. Demchenko, M.T. Halicek, M.L. Norman, M.J. Turk, T. Abel et al., *The birth of a galaxy - III. Propelling reionization with the faintest galaxies*, *MNRAS* **442** (2014) 2560 [1403.6123].
- [112] B.E. Robertson, R.S. Ellis, S.R. Furlanetto and J.S. Dunlop, *Cosmic Reionization and Early Star-forming Galaxies: A Joint Analysis of New Constraints from Planck and the Hubble Space Telescope*, *ApJ* **802** (2015) L19 [1502.02024].
- [113] R.J. Bouwens, G.D. Illingworth, P.A. Oesch, J. Caruana, B. Holwerda, R. Smit et al., *Reionization After Planck: The Derived Growth of the Cosmic Ionizing Emissivity Now Matches the Growth of the Galaxy UV Luminosity Density*, *ApJ* **811** (2015) 140 [1503.08228].
- [114] P. Dayal, M. Volonteri, T.R. Choudhury, R. Schneider, M. Trebitsch, N.Y. Gnedin et al., *Reionization with galaxies and active galactic nuclei*, *MNRAS* **495** (2020) 3065 [2001.06021].
- [115] H. Atek, I. Labbé, L.J. Furtak, I. Chemerynska, S. Fujimoto, D.J. Setton et al., *Most of the photons that reionized the Universe came from dwarf galaxies*, *Nature* **626** (2024) 975.
- [116] M. Chevallier and D. Polarski, *Accelerating Universes with Scaling Dark Matter*, *International Journal of Modern Physics D* **10** (2001) 213 [gr-qc/0009008].
- [117] E.V. Linder, *Exploring the Expansion History of the Universe*, *Phys. Rev. Lett.* **90** (2003) 091301 [astro-ph/0208512].
- [118] R.K. Sheth and G. Tormen, *Large-scale bias and the peak background split*, *MNRAS* **308** (1999) 119 [astro-ph/9901122].
- [119] A. Jenkins, C.S. Frenk, S.D.M. White, J.M. Colberg, S. Cole, A.E. Evrard et al., *The mass function of dark matter haloes*, *MNRAS* **321** (2001) 372 [astro-ph/0005260].
- [120] D.J. Eisenstein and W. Hu, *Baryonic Features in the Matter Transfer Function*, *ApJ* **496** (1998) 605 [astro-ph/9709112].
- [121] E. Sobacchi and A. Mesinger, *The depletion of gas in high-redshift dwarf galaxies from an inhomogeneous reionization.*, *MNRAS* **432** (2013) L51 [1301.6776].
- [122] J.B. Oke, *Absolute Spectral Energy Distributions for White Dwarfs*, *ApJS* **27** (1974) 21.
- [123] J.B. Oke and J.E. Gunn, *Secondary standard stars for absolute spectrophotometry.*, *ApJ* **266** (1983) 713.
- [124] C. Leitherer, D. Schaerer, J.D. Goldader, R.M.G. Delgado, C. Robert, D.F. Kune et al., *Starburst99: Synthesis Models for Galaxies with Active Star Formation*, *ApJS* **123** (1999) 3 [astro-ph/9902334].
- [125] C. Simmonds, S. Tacchella, K. Hainline, B.D. Johnson, D. Puskás, B. Robertson et al., *Ionizing properties of galaxies in JADES for a stellar mass complete sample: resolving the cosmic ionizing photon budget crisis at the Epoch of Reionization*, *MNRAS* **535** (2024) 2998 [2409.01286].
- [126] A. Pahl, M.W. Topping, A. Shapley, R. Sanders, N.A. Reddy, L. Clarke et al., *A Spectroscopic Analysis of the Ionizing Photon Production Efficiency in JADES and CEERS: Implications for the Ionizing Photon Budget*, *ApJ* **981** (2025) 134 [2407.03399].
- [127] R. Begley, R.J. McLure, F. Cullen, D.J. McLeod, J.S. Dunlop, A.C. Carnall et al., *The evolution of [O III] + H $\beta$  equivalent width from  $z = 3$ -8: implications for the production and escape of ionizing photons during reionization*, *MNRAS* **537** (2025) 3245 [2410.10988].
- [128] R.J. Bouwens, P.A. Oesch, M. Stefanon, G. Illingworth, I. Labbé, N. Reddy et al., *New Determinations of the UV Luminosity Functions from  $z = 9$  to 2 Show a Remarkable Consistency with Halo Growth and a Constant Star Formation Efficiency*, *AJ* **162** (2021) 47 [2102.07775].



- [129] C.T. Donnan, R.J. McLure, J.S. Dunlop, D.J. McLeod, D. Magee, K.Z. Arellano-Córdova et al., *JWST PRIMER: a new multifield determination of the evolving galaxy UV luminosity function at redshifts  $z = 9 - 15$* , [\*MNRAS\* \*\*533\*\* \(2024\) 3222](#) [[2403.03171](#)].
- [130] V. Mauerhofer and P. Dayal, *The dust enrichment of early galaxies in the JWST and ALMA era*, [\*MNRAS\* \*\*526\*\* \(2023\) 2196](#) [[2305.01681](#)].
- [131] N. Menci, A. Grazian, M. Castellano, P. Santini, E. Giallongo, A. Lamastra et al., *Constraints on Dynamical Dark Energy Models from the Abundance of Massive Galaxies at High Redshifts*, [\*ApJ\* \*\*900\*\* \(2020\) 108](#) [[2007.12453](#)].
- [132] P. Wang, B.-Y. Su, L. Zu, Y. Yang and L. Feng, *Exploring the dark energy equation of state with JWST*, [\*European Physical Journal Plus\* \*\*139\*\* \(2024\) 711](#) [[2307.11374](#)].
- [133] A.G. Adame, J. Aguilar, S. Ahlen, S. Alam, D.M. Alexander, M. Alvarez et al., *DESI 2024 VI: cosmological constraints from the measurements of baryon acoustic oscillations*, [\*J. Cosmology Astropart. Phys.\* \*\*2025\*\* \(2025\) 021](#) [[2404.03002](#)].
- [134] D. Brout, D. Scolnic, B. Popovic, A.G. Riess, A. Carr, J. Zuntz et al., *The Pantheon+ Analysis: Cosmological Constraints*, [\*ApJ\* \*\*938\*\* \(2022\) 110](#) [[2202.04077](#)].
- [135] T.R. Choudhury and A. Paranjape, *Photon number conservation and the large-scale 21 cm power spectrum in seminumerical models of reionization*, [\*MNRAS\* \*\*481\*\* \(2018\) 3821](#) [[1807.00836](#)].
- [136] T.R. Choudhury and A. Chakraborty, *Capturing Small-Scale Reionization Physics: A Sub-Grid Model for Photon Sinks with SCRIPT*, [\*arXiv e-prints\* \(2025\) arXiv:2504.03384](#) [[2504.03384](#)].